FACULTAD DE CIENCIAS - UNIVERSIDAD DE CHILE

CARACTERIZACIÓN DE MODELOS DE PÉRDIDA Y GANANCIA DE FUNCIÓN PARA LA FOLDASA ERP57 EN EL SISTEMA NERVIOSO CENTRAL

Seminario de Título entregado a la Universidad de Chile en cumplimiento parcial de los requisitos para optar al Título de Ingeniero en Biotecnología Molecular

CATHERINE IRIS ANDREU CAFATI

Director de Seminario de Título: Dr. Claudio Hetz Flores

Co-Directora de Seminario de Título: Dr. Ute Woehlbier

Abril, 2012

Santiago – Chile

FACULTY OF SCIENCES - UNIVERSITY OF CHILE

CHARACTERIZATION OF MOUSE MODELS OF LOSS AND GAIN OF FUNCTION FOR THE FOLDASE ERP57 IN THE CENTRAL NERVOUS SYSTEM

Seminar of Title given to the University of Chile in partial fulfillment of the requirements to qualify for the Engineering degree in Molecular Biotechnology

CATHERINE IRIS ANDREU CAFATI

Director of Seminar Title: Claudio Hetz Flores, PhD.

Co-Director of Seminar Title: Ute Woehlbier, PhD.

April, 2012

Santiago – Chile

ESCUELA DE PREGRADO – FACULTAD DE CIENCIAS – UNIVERSIDAD DE CHILE

INFORME DE APROBACIÓN SEMINARIO DE TITULO

Se informa a la Escuela de Pregrado de la Facultad de Ciencias, de la Universidad de Chile que el Seminario de Título, presentado por la Srta. Catherine Iris Andreu Cafati

"CARACTERIZACIÓN DE MODELOS DE PÉRDIDA Y GANANCIA DE FUNCIÓN PARA LA FOLDASA ERP57 EN EL SISTEMA NERVIOSO CENTRAL"

Ha sido aprobado por la Comisión de Evaluación, en cumplimiento parcial de los requisitos para optar al Título de Ingeniero en Biotecnología molecular.

Dr. Claudio Hetz Flores

Director Seminario de Título

Dr. Ute Woehlbier

Co-Directora Seminario de Título

Comisión de Evaluación

Dr. Christian González

Presidente Comisión

Dr. Miguel Allende

Evaluador

"The human mind is like a parachute, it works best when it is open".

Albert Einstein

BIOGRAFÍA

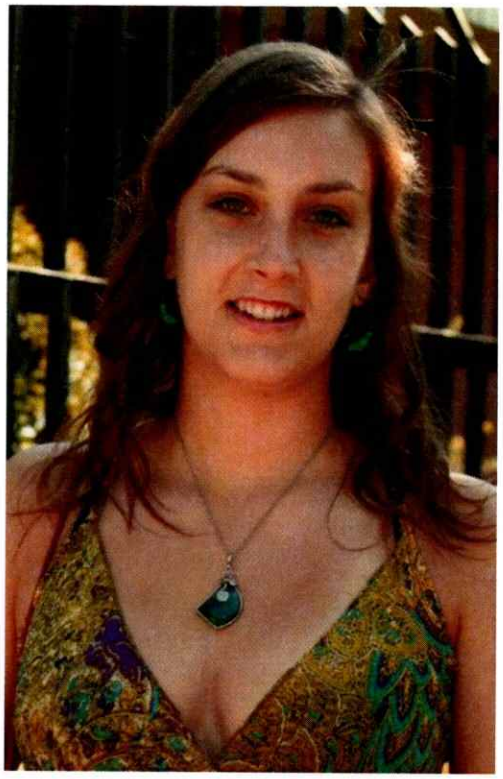

Hace 23 años, las flores primaverales me dieron la bienvenida en mi nacimiento en Santiago, lugar donde nací como la menor de tres hermanas. Desde que era pequeña, siempre fui muy curiosa con seres vivos como plantas y animales, sobretodo el misterio de cómo pueden vivir y crecer de una manera perfecta. Luego, en el colegio comencé a estudiar biología y me di cuenta que quería ser una científica. Al aprender sobre genética decidí estudiar Ingeniería en Biotecnología Molecular en la Universidad de Chile, para así poder usar las herramientas modernas con el fin de estudiar la vida. Estaba maravillada de cómo se puede entender el cerebro y así conocí el trabajo del científico chileno Francisco Varela, el cual hasta hoy sigue siendo mi fuente de inspiración. En la Universidad de Chile aprendí que significa hacer ciencia, los costos y beneficios que esto trae y que muchas veces no es una vida fácil. Además, en este hermoso y diverso campus conocí mucha gente diversa que me ayudó a abrir mi mente a los mundos y realidades distintos al mío. Aprendí de la experiencia de enseñar a estudiantes, siendo ayudante de algunos cursos de la carrera. Finalmente, ahora entiendo hacia dónde apunta mi vida, en este proceso de término de la carrera me encuentro pintando con colores un sueño en el que lentamente comienzo a caminar, aprendiendo paso a paso y encontrando en este camino a las personas necesarias para que me ayuden en él. Seguramente, tengo mucha vida por delante, en la que muchos errores y aprendizajes vendrán de ella.

AGRADECIMIENTOS

Quisiera agradecer a muchísimas personas que me han ayudado en diferentes aspectos de mi vida... ¡las palabras faltan para expresar mi agradecimiento!

Primero quisiera agradecer a mis padres Iris y Richard, quienes siempre me apoyaron en mis decisiones y estuvieron conmigo en mis momentos más difíciles. También a mis hermanas, Nicole y Denisse, quienes siempre me acompañaron cuando lo necesite.

A mis amigos del alma, por distraerme cuando necesitaba pensar en otra cosa o simplemente tener un momento agradable. Por todas las risas y lágrimas que compartimos, por todos sus consejos y todas las veces que me subieron el ánimo. Por todas nuestras aventuras juntos y simplemente por su existencia en mi vida.

A mis amigos de la Universidad, porque como un grupo nos apoyamos unos a otros durante estos 5 años, por hacerme disfrutar las clases cuando no eran tan divertidas, por compartir buenos momentos no sólo en clases, también en los recreos, después de las pruebas, en los pastos... Por tenerme paciencia para explicarme sobre plantas y microbiología, ramos que precisamente no eran mis favoritos... Agradecimientos especiales a Beatriz, Clio, Valeria, Macarena, Hernán, Matías, Ariel, Gonzalo (Talo) y Rodrigo (Rolo). Agradecimientos particulares a Ismael, por todo lo que compartimos, por todo lo que me enseñaste y me apoyaste y por el sueño científico tan especial que tenemos, ¡vamos por eso!

Quisiera agradecer a Nicolás, por estar conmigo durante todo este tiempo difícil y muy estresante, por todo lo que me has enseñado, por distraerme en los momentos más difíciles, por escucharme y aconsejarme, por hacerme reír incluso cuando no estaba de ánimo, por darme fuerza tantas veces.

Al Laboratorio de Dinámica Celular y Neuronal, por instruirme en mi primera etapa, especialmente a Cristina, Erick y Daniel por su paciencia y comprensión.

Quisiera agradecer a Claudio Hetz, por confiar en mí y apoyarme durante toda mi tesis, por aconsejarme y direccionarme en mi futuro, por enseñarme y darme la oportunidad de hacer ciencia de gran calidad.

Gracias a todos los miembros del Laboratorio de Estrés Celular y Biomedicina, por ser un gran grupo de trabajo. Particularmente a Ute Woehlbier, por ser una maravillosa tutora, por responder todas mis preguntas, por direccionarme y aconsejarme, porque siempre se hizo el tiempo para apoyarme en todo lo que necesité, por ayudarme a entender cómo funcionan las cosas fuera de Chile, por ser mi profesora particular de Inglés y un poco de Alemán, por enseñarme y por toda su paciencia. Gracias también a René Vidal, por enseñarme con su experticia en el cerebro, por muchas veces enfocarme en lo que es una tesis; a Vicente Valenzuela por su genial cooperación con los experimentos en médula espinal; Maritza Oñate, por enseñarme la técnica del Footprinting y Diego Rojas-Rivera por enseñarme sobre q-PCR y porque junto a Gabriela Martínez resultaron ser muy buenos compañeros. Además, gracias especiales a Mauricio Torres y Thergiory Irrázabal por su ayuda en la generación y mantención de las colonias y por orientarme en mi trabajo.

INDEX

FIGURE INDEX

TABLE INDEX

ABBREVIATION INDEX

ATF4	Activating transcription factor 4
BIP	Binding protein/Grp78
Bp	Base Pair
cDNA	Complementary Deoxyribonucleic Acid
cm	Centimeters
CNX	Calnexin
CRT	Calreticulin
CNS	Central Nervous System
DNA	Deoxyribonucleic Acid
DTT	Dithiothreitol
eIF2α	Eukaryotic translation initiation factor 2α
EMG	Electromyogram
ER	Endoplasmic Reticulum
ERO1	Endoplasmic Reticulum Oxidoreductase
ERp57	Endoplasmic Reticulum Protein 57/Grp58
ERp72	Endoplasmic Reticulum Protein 72
GFAP	Glial fibrillary acidic protein
h	Hours
HBSS	Hank's Balanced Salt Solution
HET	Heterozygote/ERp57$^{Nes+/-}$
HSP90	Heat shock protein 90
IU	International Units
kDa	KiloDalton
KO	Knockout/ERp57$^{Nes-/-}$
MHC	Major Histocompatibility Complex
min	Minutes
mm	Millimeters
mRNA	Messenger Ribonucleic Acid
NeuN	Neuronal Nuclei
Non-Tg	Non transgenic/ ERp57^{Non-Tg}
OCT	Optimal Cutting Temperature
PBS	Saline Phosphate Buffer
PC	Purkinje cells
PCR	Polymerase Chain Reaction
PDI	Protein Disulfide Isomerase
PDIs	PDI proteins
PFA	Paraformaldehyde
PSW	Positive Sharp Waves
qRT-PCR	Quantitative Reverse Transcriptase PCR

RNA	Ribonucleic Acid
rpm	Revolutions Per Minute
sec	Seconds
SEM	Standard Error of the Mean
SOD1	Superoxide Dismutase 1
TEMED	Tetramethylethylenediamine
Tg	Transgenic/ $ERp57^{Tg}$
UPR	Unfolded Protein Response
WT	Wildtype/$ERp57^{WT}$
XBP1	X-Box binding protein-1

1. ABSTRACT.

ERp57 is a member of the PDI family, and an ER foldase that participates in the folding of glycoproteins as part of the calnexin/calreticulin cycle. ERp57 has been related to several diseases, including cancer and hepatitis, in which its contribution is well studied. The role of ERp57 in the nervous system and its possible contribution to neurodegenerative diseases, such as Alzheimer's disease and Amyotrophic lateral sclerosis is still unclear. In this thesis, we generated and characterized a conditional *erp57* knockout and a transgenic mouse model with specific deletion or over-expression of the *erp57* gene in the central nervous system. The lack of ERp57 led to motor impairment as determined by visual observation of mice and measurements of motor coordination using Rotarod, Hanging and Footprinting tests. The cause of the motor phenotype observed was investigated by EMG measurements to detect signs of muscle denervation, which indeed were found in ERp57 deficient mice. The brain and the spinal cord were analyzed by histology. In knockout mice, a slight decrease in the motor neuron number was found in the spinal cord. Since ERp57 is an ER chaperone, protein homeostasis in different tissues was analyzed by monitoring the expression of important chaperones. Western blot analysis indicated altered expression of ERO1, calnexin, PDI, BIP and ERp72 in *erp57* knockout mice. A general decrease in all proteins analyzed was observed in cortex and cerebellum. Together, these results indicate that ERp57 has an important role in the nervous system and if deleted, motor impairment with defects in spinal cord and muscle-nerve connectivity occurs. Abnormal protein homeostasis may be the cause of the motor phenotype observed. In contrast, transgenic mice over-expressing ERp57 in brain tissues and spinal cord did not display any relevant spontaneous phenotype. However further analyses are necessary to study the effect of increased levels of ERp57 in the nervous system.

In summary, two mouse models to study ERp57 function were generated, constituting useful tools to analyze the contribution of ERp57 in the central nervous system and diseases.

2. RESUMEN.

ERp57 es una proteína miembro de la familia de las Proteínas Disulfuro Isomerasas y una foldasa del retículo endoplásmico que participa en el plegamiento de glicoproteínas, siendo parte del ciclo calnexina/calreticulina. ERp57 ha sido relacionada con diversas enfermedades, como cáncer y hepatitis, en las cuales su contribución ha sido ampliamente estudiada. El rol de ERp57 en el sistema nervioso y su posible contribución en enfermedades neurodegenerativas, como Alzheimer y Esclerosis Lateral Amiotrófica aún no ha sido dilucidado. En esta tesis, se generaron y caracterizaron ratones condicionales deficientes y transgénicos para ERp57 en el sistema nervioso central. La ausencia de ERp57 conlleva a un impedimento motor, indicado por observación visual de los ratones y mediciones de coordinación motora usando las pruebas de Rotarod, Hanging y Footprinting. La causa del fenotipo motor observado fue investigada mediante mediciones de Electromiograma para detectar la inervación del músculo, en donde se encontraron signos de denervación en ratones deficientes para ERp57. El cerebro y la médula espinal fueron analizados por histología. En ratones deficientes se encontró una leve disminución en el número de neuronas motoras de la médula espinal. Como ERp57 es una chaperona del retículo endoplásmico, se analizó la homeostasis proteica en diferentes tejidos midiendo la expresión de otras chaperonas importantes. Mediante Western blot se encontró alterada la expresión de ERO1, calnexina, PDI, BIP y ERp72 en los ratones deficientes, en los que se observó una disminución general en todas las proteínas analizadas en corteza y cerebelo. En conjunto, estos resultados indican que ERp57 tiene un rol importante en el sistema nervioso y que cuando está delecionada, se

desarrolla un impedimento motor con defectos en la médula espinal y en la conectividad del nervio con el músculo. La homeostasis proteica anormal puede ser la causa del fenotipo motor observado. Por otro lado, los ratones transgénicos que sobreexpresan ERp57 en el cerebro y la médula espinal no presentaron algún fenotipo relevante espontáneo. Sin embargo, se deben realizar análisis adicionales para estudiar el efecto de los niveles aumentados de ERp57 en el sistema nervioso.

En resumen, se generaron dos modelos murinos para estudiar la función de ERp57, constituyendo herramientas útiles para el análisis de la contribución de ERp57 en el sistema nervioso central y en enfermedades.

3. INTRODUCTION.

Neurodegenerative diseases, such as Alzheimer's disease (AD), Prion-related disorders (PrDs) and Amyotrophic lateral sclerosis (ALS) among others, are commonly associated with the accumulation of intracellular and/or extracellular aggregates of misfolded protein in the brain (Matus et al., 2011) . The cellular processes underlying disease pathogenesis are not well understood. In recent years, accumulating evidence suggest that the capacity of the endoplasmic reticulum (ER) to maintain protein homeostasis is an important factor in these protein folding disorders. The ER contains a complex network of protein chaperones, foldases, and co-factors that catalyze oxidative protein folding and prevent abnormal protein aggregation. ERp57 is an ER foldase that is involved in the calnexin/calreticulin cycle and is a member of the Protein Disulfide Isomerase (PDI) family (Khanal and Nemere, 2007). ERp57 has been related with the occurrence of some neurodegenerative diseases (Coe and Michalak, 2010) although its role in the nervous system *in vivo* has not been explored yet.

3.1. Endoplasmic reticulum, ER stress, and the UPR.

The ER is a cellular compartment where 30% of proteins are initially folded, matured and trafficked through the secretory pathway. ER resident chaperones, foldases and co-factors participate in protein folding in the ER lumen, preventing protein misfolding and aggregation thereby maintaining cellular function (Hetz, 2012). Several types of cellular damage cause disturbance of ER-related processes and chaperone function, resulting in accumulation of unfolded or misfolded proteins within the ER, causing a cellular condition referred to as "ER stress". ER stress triggers the activation of the unfolded protein response (UPR), an integrated signaling cascade pointing to the adaptation of cellular processes to re-establish cellular homeostasis (Walter and Ron, 2011). In the first place,

the UPR increases the capacity of the ER to fold proteins through an up-regulation of the expression of several ER chaperones, such as BIP, Grp94, calreticulin, calnexin and PDI proteins (PDIs). The UPR also regulates genes involved in quality control, protein degradation by autophagy and other aspects of the secretory pathway. In addition, the removal of misfolded proteins from the ER via ER-associated degradation (ERAD) is stimulated, where proteins are retro-translocated to the cytosol and degraded by the ubiquitin-proteasome system (UPS) (Schroder and Kaufman, 2005).

A triade of ER transmembrane proteins acts as stress sensors and activate the UPR: inositol requiring kinase 1 (IRE1) including IRE1α and IRE1β, activating transcription factor 6 (ATF6) and PKR-like ER kinase (PERK) (Figure 1). These proteins are responsible for monitoring the protein folding capacity of the ER and transduce the information to the cytosol and nucleus, thereby controlling the expression of specific transcription factors and signaling events (Hetz et al., 2011). If the mechanisms of adaptation triggered by the UPR are insufficient to recover homeostasis, the cell enters in a phase of chronic ER stress and switches to an opposing cascade of events leading to cellular death by apoptosis. Chronic ER stress is described in the symptomatic and late stage of many neurodegenerative diseases, including AD, Parkinson´s disease (PD), Hungtinton´s disease (HD), PrDs and ALS (Matus et al., 2011).

In the UPR pathway, summarized in Figure 1, IRE1α is a protein kinase and endoribonuclease that modulates the unconventional splicing of X-Box binding protein-1 (XBP1) mRNA, producing a more stable protein, XBP1s, which induces the transcription of UPR-related genes that function in protein quality control, folding, ERAD and ER and Golgi biogenesis (Ron and Walter, 2007). IRE1α also has additional functions in cell signaling, like the activation of Apoptosis Signal-regulating Kinase 1 (ASK1) and c-Jun-N terminal kinase (JNK), and in the modulation of the autophagy levels, an important mechanism to

eliminate aggregated proteins and damaged organelles (Rubinsztein et al., 2011). ATF6 activation results in its translocation to the Golgi, where it is processed releasing its cytosolic domain which functions as a transcription factor that modulates the expression of ER chaperones, ERAD-related genes and XBP1 (Chen et al., 2002) . PERK phosphorylates eIF2α, a translation initiation factor that inhibits translation into the ER. This leads to increased levels of the transcription factor ATF4, which controls UPR-target genes encoding proteins involved in redox homeostasis, amino acid metabolism, apoptosis and autophagy (Harding et al., 2003).

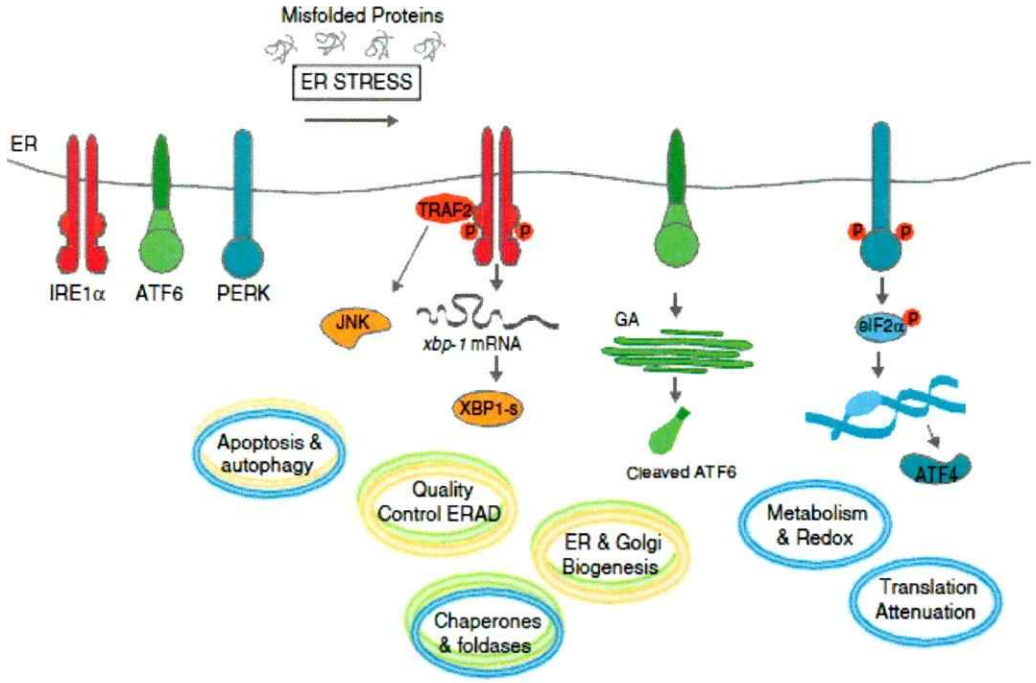

Figure 1. UPR signaling pathways. The accumulation of misfolded proteins in the ER leads to the activation of the UPR through three sensors: IRE1α, ATF6 and PERK, which triggers signaling cascades to restore cellular homeostasis or to activate the pathway of cell death by apoptosis. Modified from Matus et al., 2011.

3.2. Protein Disulfide Isomerase family.

Some PDI family members have been reported to be regulated by the UPR, including PDI, ERp57 and ERp72 (Dorner et al., 1990; Maattanen et al., 2010).

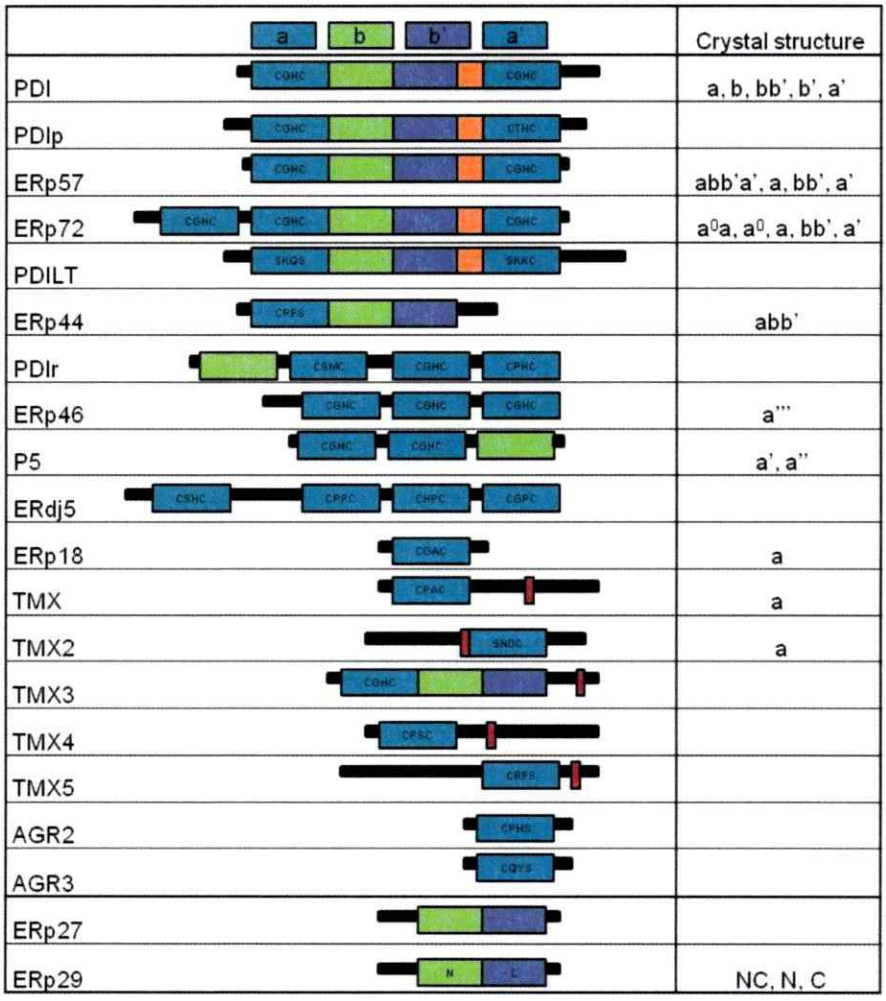

Figure 2. Members of the PDI family. The list of the 20 members of the PDI family with their structure by domain and the crystal structure that has been solved is shown. PDI and ERp57 presented a similar domain structure. In blue, catalytic domains "a" and "a'" are shown. Non-catalytic domains "b" and "b'" are colored in green and purple, respectively. In orange the x-linker between "b'" and "a'" is shown.

PDIs are a protein family comprised of approximately 20 members of the thioredoxin superfamily (Figure 2), which are predominantly located to the ER. The ER lumen provides the most favorable environment for disulfide bond formation since it is relatively more oxidizing than the cytosol (Feige and Hendershot, 2011). Disulfide bonds in proteins are produced by the oxidation of two free thiols originating from two cysteine residues. The presence of disulfide bonds within (intramolecular) and between (intermolecular) proteins has important implications for the stability of the structure of proteins or protein complexes.

In addition, disulfide bonds may act as regulatory switches providing a mechanism to control the function of proteins or protein complexes (Feige and Hendershot, 2011). Disulfide bond formation is a critical step in the maturation of many of the proteins transversing the ER. However, PDIs not only act as foldases, in addition they perform essential functions as molecular chaperones by inhibiting the aggregation of misfolded proteins that do not contain disulfide bonds (Ferrari and Soling, 1999; Grubb et al., 2012; Maattanen et al., 2010; Turano et al., 2002). PDI family members contain a modular domain-structure including thioredoxin-like catalytic "a" domains, and non-catalytic "b" domains. The PDI family also contains thiol-reactive (e.g. PDI, PDIp, ERp57, ERp72) and non-reactive members (ERp27 and ERp29) (Kozlov et al., 2010).

PDI was the first PDI family member identified and is the best described in the literature. Data derived from structural and functional studies of PDI therefore dominate the view of PDIs today. PDI itself contains four domains in the following order "a", "b", "b'" and "a'" (Kozlov et al., 2010). The catalytic "a" domains contain CXXC active-site motifs that react with thiols of newly synthesized proteins and determine the redox potential of PDI and its role as a reductase, oxidase or isomerase (Kozlov et al., 2010). In an oxidized state, the disulfide can be transferred to the substrate to catalyze its oxidation and the active site becomes reduced. Conversely, in a reduced state the disulfide of the substrate can be reduced and the active site becomes oxidized again (Ellgaard and Ruddock, 2005). The non-catalytic "b" domains act as spacers and are responsible for substrate recruitment (Denisov et al., 2009). A 19 aminoacid linker region (x-linker) was described to provide more flexibility between the b' and a' domain (Pirneskoski et al., 2004), thereby modulating substrate binding capacity. PDIs also can catalyze the rearrangement (isomerization) of incorrectly formed disulfides. Isomerization consist of cycles of reduction and oxidation (Appenzeller-Herzog and Ellgaard, 2008).

The redox state of PDI and other PDI family members in the ER is presumably directly influenced by the glutathione redox buffer consisting of reduced glutathione (GSH) and oxidized glutathione (GSSG), as well as the presence and kinetics of other oxidases, reductases and substrates (Hatahet and Ruddock, 2009). However, a major pathway for disulfide bond formation in the ER is attributed to the FAD-binding oxidases ERO1α and ERO1β (Feige and Hendershot, 2011; Tu and Weissman, 2002). The cycle of oxidation and transfer of electrons between substrates of PDIs, PDIs and ERO1 is shown in Figure 3, finally leading to the production of hydrogen peroxide (Tu and Weissman, 2002) .

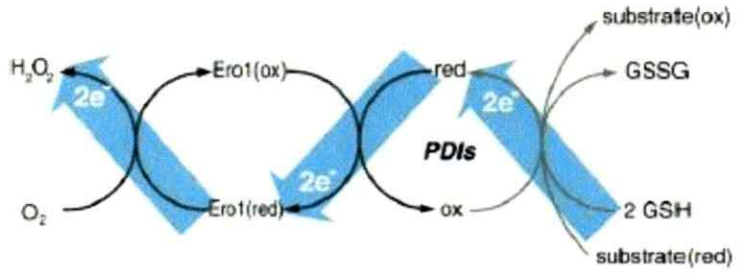

Figure 3. Electron flow pathways present in the cycle of PDI activity. Reduced PDIs can be oxidized by oxidized ERO1 that finally transfers the electrons to molecular oxygen, producing hydrogen peroxide. Oxidized PDIs can react with reduced substrates or GSH. Red: reduced, ox: oxidized, GSSG: oxidized glutathione, GSH: reduced glutathione. Modified of Appenzeller-Herzog and Ellgaard, 2008.

Depletion of PDI in cells results in a delay in disulfide bond formation of secretory proteins highlighting the role of PDI in oxidative protein folding (Rutkevich et al., 2010). PDI has wide substrate specificity, whereas ERp57, the closest homologue of PDI, is proposed to have a more refined substrate clientele (Feige and Hendershot, 2011).

Each PDI family member displays diverse structural and functional properties. Together PDIs fulfill key roles as ER foldases and chaperones, thereby promoting native protein folding, and actively participate in ER related processes. In addition, PDIs function as molecular chaperones preventing protein misfolding and aggregation. PDIs and related proteins also have been linked to some neurodegenerative diseases (Benham, 2012;

Matus et al., 2011), where their involvement in various pathogenic mechanisms and their function is still undefined.

3.3. PDIs and neurodegeneration.

Neurodegenerative diseases including AD, PD, HD, PrDs and ALS are pathologies that can affect diverse functions of the nervous system like movements, emotions, cognition, memory, thinking processes and other abilities (Soto, 2003). The accumulation of misfolded and aggregated proteins in the brain is a common factor in these diseases (Mukherjee and Soto, 2011) and leads to neurodegeneration characterized by the disturbance of basic neuronal functions, including axonal transport, synapse formation and maintainance, resulting in oxidative stress, proteasome inhibition, neuronal loss and finally brain dysfunction (Jellinger, 2010).

PDIs have been related to several neurodegenerative diseases, as summarized in Table 1. By proteomic analysis, ERp57 and PDI were identified as two major up-regulated proteins in spinal cords of mutant SOD1 transgenic rat and mouse ALS models (Atkin et al., 2006; Massignan et al., 2007). This is consistent with the increased expression of ERp57 and PDI found in spinal cord and the CSF of sporadic ALS patients (Atkin et al., 2008; Hetz et al., 2009). In the brains of Creutzfeldt–Jakob (CJD) patients, ERp57 was found to be up-regulated (Hetz et al., 2003; Yoo et al., 2002), as it was in the brains of mice infected with the scrapie strain 139A (Hetz et al., 2005). ERp57 was found to interact with β-amyloid in AD (Erickson et al., 2005) suggesting a role as a carrier protein which prevents aggregation of the β-amyloid peptide. In addition, PDI is present in neurofibrillary tangles of brain tissues of AD patients (Honjo et al., 2010). Knockdown of PDI in the motoneuron like NSC-34 cell line increased the level of mutant SOD1 inclusions and over-expression of PDI decreased mutant SOD1 aggregation, toxicity and ER stress (Walker et al., 2010). In addition, S-nitrosylated PDI, an enzymatically inactivated form of the protein,

was found in the spinal cords of ALS patients and SOD1 transgenic ALS mice (Walker et al., 2010), as well as in the brains of PD and AD patients (Uehara et al., 2006). Knockdown of ERp57 in N2a neuroblastoma cells resulted in an increased scrapie prion (PrP^{SC}) toxicity and conversely over-expression of ERp57 conferred resistance to PrP^{SC} and decreased the rate of caspase-12 activation (Hetz et al., 2005). Together, these results indicate a protective role of PDIs in neurodegenerative diseases, attenuating mutant SOD1, PrP^{SC} and β-amyloid toxicity.

Table 1. PDIs in neurodegenerative diseases. Summary of the evidence presented that relates PDIs with neurodegeneration, indicating either a neuroprotective or a pro-apoptotic effect. The disease, the effect and the corresponding reference is showed.

Disease	Effect	Reference
ALS	PDI and ERp57 are up-regulated in $SOD1^{G93A}$ rats, mice, and in sporadic ALS patients	(Atkin et al., 2006; Hetz et al., 2009; Massignan et al., 2007)
	PDI knockdown increased mutant SOD1 inclusion levels and over-expression decreased inclusion levels.	(Walker et al., 2010)
	S-nitrosylated PDI is detected in ALS patients and $SOD1^{G93A}$ mice.	(Walker et al., 2010)
Parkinson	S-nitrosylated PDI was found in the brains of PD patients.	(Uehara et al., 2006)
Alzheimer	ERp57 interacts with β-amyloid preventing its aggregation.	(Erickson et al., 2005)
	PDI was present in neurofibrillary tangles.	(Honjo et al., 2010)
	S-nitrosylated PDI is detected in the brains of AD patients.	(Uehara et al., 2006)
	Inhibition of PDI and ERp57 protects against neurodegeneration related to amyloid precursors.	(Hoffstrom et al., 2010)
Creutzfeldt-Jakob	PDI is over-expressed in brains of CJD patients and ERp57 in the murine scrapie strain 139A.	(Hetz et al., 2003; Yoo et al., 2002)
	Knockdown of ERp57 increases PrP^{SC} toxicity and over-expression confers resistance.	(Hetz et al., 2005)
Huntington	Inhibition of PDI and ERp57 suppress neuronal degeneration associated to polyglutamines.	(Hoffstrom et al., 2010)

On the other hand, PDI has been described as a pro-apoptotic factor. Several stress events, for example DNA damage, ER stress, loss of cell adhesion and cytoskeletal damage, can lead to apoptosis, a cell death program which is important to eliminate dysfunctional cells (Chipuk et al., 2006). Bcl-2 proteins regulate apoptotic signaling, including pro-apoptotic and anti-apoptotic functions, from different sub-cellular localizations including ER, mitochondria and nuclear envelope (Germain and Shore, 2003; Rodriguez et al., 2011). Bcl-2 pro-apoptotic proteins cooperate to permeabilize the mitochondrial outer membrane (MOM) causing the release of apoptogenic factors to the cytosol which activate caspases (Tait and Green, 2010). In a recent publication, it was described that Bcl-2 proteins can also regulate the ER membrane permeability to luminal proteins during apoptosis (Wang et al., 2011). PDI and BIP were detected in cytosolic fractions of wildtype cells treated with ER stressors like thapsigargin and tunicamycin that induce apoptosis (Wang et al., 2011). PDI may then induce mitochondrial outermembrane permeabilization (MOMP) leading to the release of proteins like cytochrome c from the intermembrane space and then the activation of caspase enzymes resulting in apoptosis (Hoffstrom et al., 2010). Also, it has been described that several compounds that inhibit PDI and ERp57 can suppress neuronal degeneration associated with polyglutamine in HD or amyloid precursor protein in AD (Hoffstrom et al., 2010). The pro-apoptotic function of PDI offers a new link between protein misfolding and cell death, which may be especially important in some disease processes and neurodegenerative pathologies that are related with misfolded proteins and apoptosis.

3.4. ERp57 – a multi-functional protein.

ERp57 also referred to as Grp58, ERp60 or Pdia3, is a 58-kDa glycoprotein-specific thiol oxidoreductase located to the ER. The human *erp57* gene consists of 13 exons and 12 introns with a length of 18 kb, located in chromosome 15q15, coding for a 505 aminoacid protein (Koivunen et al., 1997). The homologous gene in mouse maps to chromosome 2 (Khanal and Nemere, 2007). ERp57 is expressed in liver, lung, placenta, pancreas and kidney, and has a low basal expression in heart, skeletal muscle and brain (Koivunen et al., 1997).

ERp57 is involved in multiple functions in the cell; however, the main function of ERp57 has been attributed to ER protein quality control. ERp57 substrates are heavily glycosylated and disulfide bonded proteins that show common structural domains (Jessop et al., 2007). As a component of the calnexin (CNX) - calreticulin (CRT) cycle, ERp57 therefore promotes the correct disulfide formation and isomerization in glycoproteins that are entering into the CNX/CRT cycle (Figure 4) and are attached to CNX or CRT, two ER chaperones (Ellgaard and Frickel, 2003). The association of ERp57 with the CNX/CRT cycle suggests a specific role for ERp57 in the isomerization of non-native disulfide bonds in specific glycoprotein substrates (Jessop et al., 2007). In the cycle, the polypeptide binds to CNX/CRT and ERp57 to promote its folding, then is exported to Golgi or if is not correctly folded the cycle is repeated. Misfolded glycoproteins finally go to the ERAD (Figure 4). Also, in the immune system, ERp57 was reported to play a structural role in the peptide-loading complex (PLC) of major histocompatibility complex (MHC) class I molecules (Appenzeller-Herzog and Ellgaard, 2008). ERp57 also performs functions outside of the ER. For example, it has been found to localize to the nucleus, cytoplasm and cell surface (Coppari et al., 2002). ERp57 is capable of sequestering active or inactive signal transducer and activator of transcription 3 (STAT3) playing a role in the regulation of

its signaling (Coe et al., 2010). Some of the multiple roles of ERp57 in the ER, described recently, are depicted in the Figure 5.

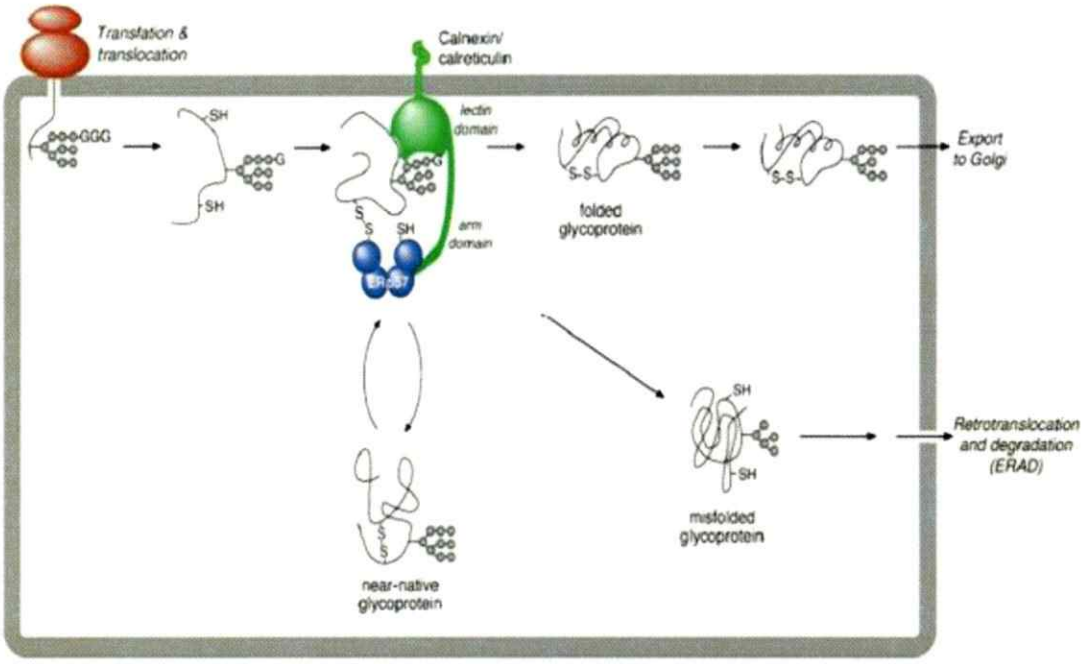

Figure 4. CNX/CRT cycle and the participation of ERp57. The folding polypeptide binds to CNX/CRT to delay folding, prevent aggregation and retain folding intermediates in the ER with the associated ERp57, promoting disulfide formation and isomerization. The glycoprotein then is finally exported to Golgi or if is not fold correctly re-binds to CNX/CRT until is correctly folded. Misfolded glycoproteins with prolonged stay in the cycle finally goes to the ERAD. G= glucose; gray sphere= mannose. Modified of Rutkevich and Williams, 2011.

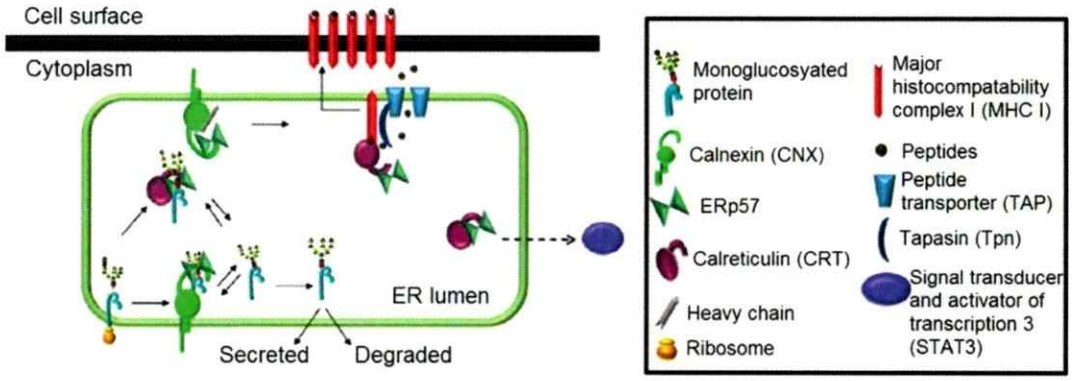

Figure 5. Different functions of ERp57 in the endoplasmic reticulum. ERp57 has a role in quality control binding to CNX (light green) and CRT (purple), also in processing of major histocompatability complex class I (red daggers) and modulates STAT3 signaling (bright purple) from the ER lumen. Adapted from Coe and Michalak, 2010.

Eventhough ERp57 has the highest sequence homology to PDI compared to other PDI family members its structure is very different from PDI (Maattanen et al., 2006). The crystal structure of yeast PDI showed a U-shaped conformation with the "a" and "a'" domains towards the middle of the U and hydrophobic residues on the inside of the U (Tian et al., 2006). The "b" and "b'" domains of PDI were also shown to form a rigid base, whereas the "a" domain is mobile (Tian et al., 2008). Several NMR structures showed that the "b'" domain of PDI has a large substrate binding site with residues for the recognition of unfolded proteins, the "b" domain was found to be important for the regulation of substrate binding of the "b'" domain which also can be blocked by the x-linker region (Rutkevich and Williams, 2011). ERp57 on the other hand, contains a group of positively charged residues in the "b'" domain that interacts with a negatively charged region of CNX and CRT. The hydrophobic area in this "b'" domain in PDI is absent in ERp57 (Kozlov et al., 2006). The crystal structure of ERp57 with tapasin, a supporting protein during the peptide loading of MHC class I molecules, revealed that "a" hydrophobic areas close to the ERp57 active sites regulates the interaction of ERp57 with tapasin (Dong et al., 2009). This suggests that these regions are the structural basis for substrate interaction which are also present in PDI and ERp72 (Rutkevich and Williams, 2011). Also, it has been described that in cells deficient in ERp57, ERp72 could compensate for the loss of its function and may associate with substrates of ERp57 to maintain their folding (Solda et al., 2006).

3.5. ERp57 function in the nervous system.

ERp57 has been related to diseases such as cancer, where it is over-expressed in transformed cells (Hirano et al., 1995), playing a role in oncogenic transformation and in modulation of STAT3 signaling proliferation (Coe et al., 2010; Guo et al., 2002). In liver diseases, ERp57 was found to be trifloroacetylated during liver failure abolishing its function in quality control, resulting in liver toxicity (Khanal and Nemere, 2007). Although

ERp57 also has been related with many different neurodegenerative diseases, the possible role of ERp57 in the nervous system is still unknown. Interestingly, ERp57 was suggested to be a useful biomarker for the disease progression in ALS by using peripheral blood mononuclear cells (PBMC) of human patients and $SOD1^{G93A}$ transgenic rats (Nardo et al., 2011).

In summary, the studies that relate ERp57 with neurodegeneration point towards the importance of this protein as an interesting target for future development of treatments and early diagnosis of diseases. Many questions about the biology of PDIs remain to be answered, specifically relating their structures with their individual functions. More importantly, additional studies are required to define the role of PDIs in protein folding and in specific disease contexts *in vivo*.

3.6. Mouse models to study PDIs and ER chaperones.

To date, only few knockout mouse models for PDIs have been described, including ERp57, ERdj5 and AGR2 (Coe et al., 2010; Garbi et al., 2006; Hosoda et al., 2010; Nemere et al., 2010; Park et al., 2009; Zhao et al., 2010). In addition, none has so far analyzed the function of PDIs in the brain. ERdj5 was found to contribute to salivary gland ER protein quality control (Hosoda et al., 2010). AGR2, anterior gradient homolog 2, was shown to have a specific role in intestinal mucus production (Park et al., 2009), and in intestinal homeostasis in addition to the etiology of inflammatory bowel disease (Zhao et al., 2010).

In the case of ERp57, the complete knockout in mice was lethal at embryonic day 13.5, possibly due to STAT3 signaling modulation (Coe et al., 2010). Deletion of ERp57 had no effect on ER morphology, ER stress, apoptosis or expression of other ER chaperones in immortalized mouse embryonic fibroblasts (MEF) cells, however STAT3-dependent signaling was increased in absence of ERp57 in MEF cells (Coe et al., 2010). In this study,

the mice expressing β-galactosidase under the control of the ERp57 promoter showed expression in the lung and liver and in later stages in the brain. A B cell specific ERp57 knockout mouse was generated employing the cre-lox system. Transgenic mice with loxP site flanked ERp57 were crossed with mice expressing cre recombinase under the control of the CD19 promoter (Garbi et al., 2006). These mice showed decreased MHC class I expression and suboptimal peptide loading in B cells, leading to impaired peptide loading complex assembly of MHC class I (Garbi et al., 2006). In addition, intestinal ERp57 knockout mice were generated crossing loxP-flanked ERp57 mice with mice expressing villin-driven cre recombinase. Intestinal cells from these knockout mice showed a severely absent response to steroid (Nemere et al., 2010). Enterocytes failed to display steroid hormone-stimulated c-AMP dependent protein kinase (PKA) activity, which normally mediates calcium uptake; but responded to forskolin with an increased calcium uptake, suggesting a role of ERp57 in steroid-stimulated calcium uptake in intestinal cells (Nemere et al., 2010).

With respect to other ER chaperones, mouse models deficient in CNX and BIP are available. A CNX knockout mouse was generated by targeted disruption of the *cnx* coding sequence. Full CNX deficient mice showed a normal development, but were smaller than their wildtype littermates and presented obvious motor disorders, including truncal ataxia, tremor, negative geotaxis and retropulsion (Denzel et al., 2002). No changes in the knockout mice were observed at the histological level of all organs and of the central and peripherial nervous system. The motor disorders were related to a significant loss of large to medium myelinated nerve fibers (Denzel et al., 2002). It is important to mention that CNX cannot compensate the loss of CRT, since CRT knockout mice die in utero between 12 to 18 days after gestation, due to a failure to absorb the umbilical hernia and defective heart development (Mesaeli et al., 1999) and conversely, CRT cannot compensate the

loss of CNX (Denzel et al., 2002). Another knockout mouse model for CNX was generated but in this case with another strategy, by gene trapping. In this model CNX-deficient mice showed demyelination indicated by electron microscopy analysis of spinal cord and sciatic nerve and reduced conductive velocity of nerve fibers. The myelin sheets in the knockout mice were decompacted and disorganized (Kraus et al., 2010).

BIP is the most abundant ER chaperone with multiple roles in the ER (Maattanen et al., 2010; Ni and Lee, 2007), regulating the UPR, functioning in quality control of protein folding (Luo et al., 2006), regulating calcium homeostasis and interacting with the three UPR sensors (Hetz, 2012). BIP also has been related with a pro-survival role in neurodegenerative diseases (Kim et al., 2011). A cerebellar Purkinje cell (PC)-specific BIP knockout mouse was generated with the cre recombinase loxP site system. These BIP-deficient mice showed accelerated degeneration of the PC and cerebellar atrophy and also presented strong motor coordination defects. These mice showed a reduction in the body weight and food consumption, bad rotarod performance and altered measurements in footprinting tests (Wang et al., 2010). It has been described that BIP knockout mice have an activated UPR, indicated by higher levels of proteins like PDI, CHOP, GRP94 and GADD34 as well as a suppression of eIF2α phosphorylation and increased apoptotic cell death, together with ER morphological alterations and a decrease in ubiquilin-protein levels and the autophagy-related protein p62 (Wang et al., 2010). Also, a spontaneous recessive mouse mutation called woozy (wz) was described affecting the ER protein folding machinery. By genome mapping, northern blot analysis and RT-PCR, SIL1 was identified as the mutated protein in these mice. SIL1 is a nucleotide exchange factor of BIP, regulating its functional recycling (Zhao et al., 2005). Homozygous wz mice developed ataxia and PC loss, accompanied by ER stress and abnormal accumulation of ubiquitinated proteins in PC (Zhao et al., 2005).

To investigate the function of ERp57 in the central nervous system (CNS), we developed a knockout and a transgenic animal to manipulate ERp57 levels specifically in the nervous tissue.

4. HYPOTHESIS.

ERp57 deficiency in the nervous system triggers motor dysfunction associated with abnormal protein homeostasis.

5. AIMS.

5.1. General Aim.

To study the possible effects in motor coordination of ERp57 deficiency and ERp57 over-expression in the nervous system of mice.

5.2. Specific Aims.

- To generate and a conditional knockout and a transgenic mouse model for ERp57 and confirm the functionality of the strategy.
- To characterize the conditional knockout and transgenic mouse model for ERp57 by monitoring visual observations, body weight measurements and motor performance by Rotarod, Hanging and Footprinting tests.
- To determine the muscle innervation in *erp57* conditional knockout mouse by Electromyography.
- To perform histological analysis of brain and spinal cord of the *erp57* conditional knockout mouse.
- To analyze the possible effect of the ERp57 deletion on the levels of other ER chaperones and PDI family members by Western blot analysis of mouse tissue.

6. MATERIAL AND METHODS.

6.1. Generation of a CNS *erp57* conditional knockout mouse model.

The ERp57 floxed mice with mixed background C57BL/6 and BALB/c were previously described (Garbi et al., 2006) and were kindly provided by Dr. Günther Hämmerling (German Cancer Research Center, Heidelberg, Germany). Mice expressing Cre recombinase under the control of the nestin promoter with a C57BL/6 background were obtained from The Jackson Laboratory (B6.Cg-Tg(Nes-cre)1Kln/J,003771). To generate CNS specific ERp57 knockout mice, ERp57 floxed mice were crossed with Nestin-cre mice and generated offspring carrying the floxed or knockout allele in heterozygous or homozygous form from hereon called $ERp57^{WT}$ (wildtype), $ERp57^{Nes+/-}$ (heterozygous), $ERp57^{Nes-/-}$ (knockout) respectively (Figure 6) with mixed background. Mice were maintained in the facilities of the University of Chile (Santiago, Chile). All experiments and animal care follows the Institutional Review Board´s Animal Care of the University of Chile (CBA # 0305 FMUCH).

Pups were weaned at 21 days of age and genotyped by PCR using the following primers: *erp57* floxed forward 5'-CGCCAGCCTCTCCATTTAG -3', *erp57* floxed reverse 5'-CAGAGATCCTGCCTCTG -3'. The PCR product observed for the littermates (wildtype) is 200 bp and for carriers of the floxed allele 387 bp. For cre recombinase the following primers were used: cre forward 5'-GCGGTCTGGCAGTAAAAACTATC -3' and cre reverse 5'-GTGAAACAGCATTGCTGTCACTT -3' to obtain a 100 bp product. Primers for IL-2 were used as a control: IL-2 forward 5'-CTAGGCCACAGAATTGAAAGATCT -3' and IL-2 reverse 5'-GTAGGTGGAAATTCTAGCATCATCC -3' resulting in a 324 bp product. For DNA extraction, a 5 mm mouse tail piece was cut and incubated with 600 µL of lysis buffer (50 mM Tris pH 8.0, 100 mM EDTA, 100 mM NaCl and 1% SDS) and 6 µL of 10 mg/mL

proteinase K for 16 h at 55°C followed by centrifugation for 5 min at 13000 xg. The supernatant was mixed with 450 µL of 100% isopropanol and the DNA was observed as a white precipitate. The pellet was washed with 1 mL of 70% ethanol, resuspended in 300 µL of TE buffer (10 mM Tris-Cl pH 7.5, 1 mM EDTA) and incubated 2 h at 55°C to facilitate homogenization. For PCR 1 µL of DNA was incubated with 12.5 µL of Go Taq Master Mix (Promega) and 1 µM of primers each in a final volume of 25 µL. The PCR program used was one cycle of denaturation for 2 minutes at 95°C, 35 cycles of 20 sec at 95°C, 20 sec at 50°C, 15 sec at 72°C and a final cycle of elongation for 3 min at 72°C. PCR products were analyzed by agarose gel electrophoresis using 1% agarose gels with 1 µg/mL ethidium bromide at 100 V.

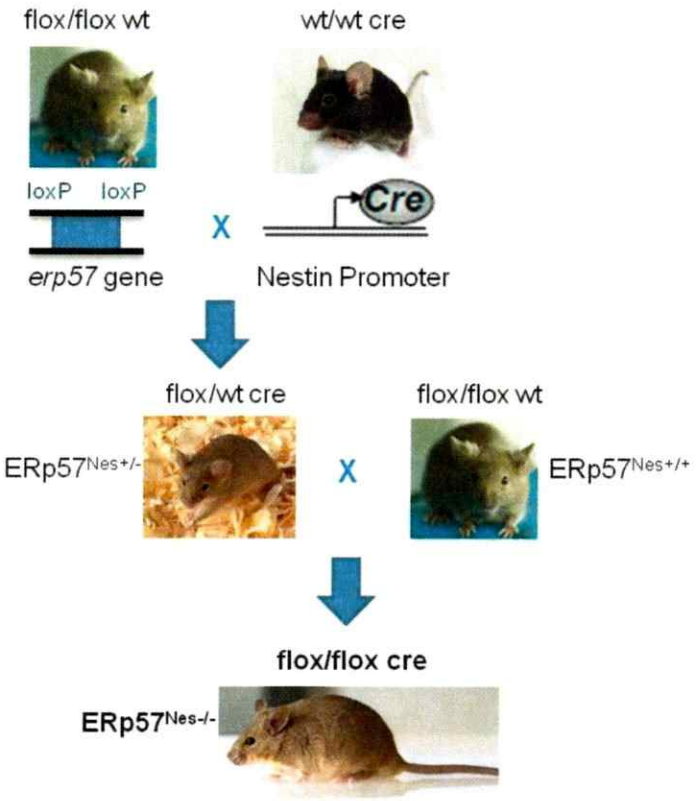

Figure 6. Strategy used to generate an *erp57* conditional knockout mice. Mice with the lox-P sites flanking the *erp57* gene (flox/flox wt) were crossed with mice that expressed the cre recombinase under the control of the nestin promoter (wt/wt cre). Of this breeding, heterozygous mice were obtained (flox/wt cre) and then crossed with flox/flox wt mice to obtain the *erp57* conditional knockout mice (flox/flox cre).

6.2. Motor and Behavioral Test.

6.2.1. Rotarod Test.

For the basic Rotarod test mice were placed into a rod rotating (Model LE8500, Panlab SL) at a constant speed of 4 rpm. The time until mice fell from the rod was measured with the maximum time being 120 sec. Previous to measurements mice were trained 3 times per day for 5 consecutive days. The measurement was done once per week.

For accelerated speed tests, animals were tested in four trials per day for two consecutive days. The tests was started with 4 rpm and increased to 40 rpm after 300 sec, the time until mice fell from the rod was measured.

6.2.2. Body weight measurements.

The body weight of mice was measured weekly beginning at 31 days until 178 days of age or from 38 days to 69 in $ERp57^{WT}$, $ERp57^{Nes+/-}$ and $ERp57^{Nes-/-}$ or $ERp57^{Tg1}$, $ERp57^{Tg5}$ and $ERp57^{Non-Tg}$ respectively.

6.2.3. Hanging Test.

Individual mice were placed hanging with their forepaws on a horizontal bar with a length of 39 cm and a height of 35 cm. The reaction of the mouse and the body position was observed for 30 seconds and recorded with a video-camera. The test was performed 3 times in one day once per week. A score was derived from each video and averaged for the three measurements done at the same day. A score of 0 was given when the mouse could not hold onto the bar for more than 10 sec, a score of 1 when the mouse maintain itself on the bar with the forelimbs, a score of 2 if the mouse maintain itself with the forelimbs and tried to use its hindlimbs but without success, a score of 3 if the mouse used

the forelimbs and one or two of the hindlimbs, a score of 4 if the mouse used all four limbs and the tail and 5 if the mouse actively escape of the bar in less than 30 sec.

6.2.4. Footprinting Test.

The forelimbs and hindlimbs of the mouse were painted with nontoxic dyes red and black, respectively. Then the mouse was placed to run in a narrow tunnel with white paper at the bottom (of 28 cm length and 11 cm width). A dark box was put at the end of the tunnel to encourage the mouse to finish the task as fast as possible. If the mouse stopped on the way the measurement was discarded and repeated. The first and the last 10 cm of the print were excluded from the analysis. The test was performed at least 4 times on one day per week. A minimum of six steps was analyzed for each measurement. The angle of rotation was measured as the angle made by two lines connecting the third toe and the stride line at the center of the paw pad. For interlimb coordination, the distance between the center pads of the ipsilateral forelimb and hindlimb was measured, as described previously in (Karimi-Abdolrezaee et al., 2006). For distance between limbs, the distance from one hindlimb to the next one was measured.

6.3. Needle Electromyography (EMG).

Animals were anesthetized with avertin, and placed in a prone position on a thermal pad at 37°C for the examination. EMG recordings using a Viking Quest portable EMG machine (Nicolet) were obtained using a 27-gauge, Teflon-coated, monopolar needle electrode with a 70 x 500 µm recording surface (PRO-37SAF; Electrode Store). A 29-gauge reference needle electrode (GRD-SAF; Electrode Store) was inserted subcutaneous in close approximation to the recording electrode. A subdermal ground electrode was placed on the back. The recording electrode was inserted into the tibialis anterior or gastrocnemius/soleus muscles, and spontaneous electrical activity was recorded for 90 sec. The system of scoring was the following: 0 is a normal activity of the

muscle, where there are no positive sharp waves (PSW) observed in any muscle analyzed; +1 is when there is a signal of PSW in some muscles, not in all analyzed; +2 is if PSW are observed in many muscles, not in all analyzed and +3 when PSW are found in all the muscles that are analyzed and it is not necessary to search for it.

6.4. Histological analysis of spinal cord and brain tissue.

6.4.1. Mouse perfusion and tissue slices.

At 60-180 days of age mice were deeply anesthetized by intraperitoneal injection of 33 µL of 10 mg/mL avertin in 0.1 M PBS per gram of body weight and perfused transcardially with 20 mL of 0.9% NaCl followed by 20 mL of cold 4% PFA in PBS pH 7.4.

A 5 mm region of the spinal cord was removed and post-fixed for 3 hours in 4% PFA. Then, the spinal cord tissue was subjected to a sucrose gradient (5%, 10% and 20% sucrose in PBS for 1 h each), cryoprotected with OCT (Optimal Cutting Temperature) and fast frozen using liquid nitrogen. The tissue was transversally sectioned (20 µm thick slices) using a cryostat microtome (Leica CM 1510S).

Brains were extracted, fixed in 4% PFA for 16 h at 4°C and subjected to a sucrose gradient (10%, 20% and 30% sucrose in PBS with 0.002% sodium azide for 1 h each) and maintained at 4°C. One brain hemisphere was mounted in an low melting point agarose block and was sagittally cut in 50 µm thick slices from lateral to medial in a vibratome (Leica VT 1000S). All the slices were collected and stored in 1X PBS at 4°C.

6.4.2. Immunofluorescence analysis.

Spinal cord sections were mounted in a VWR Micro Slides Superfrost Plus glass (VWR International) and washed 3 times with PBS for 5 min each. The slices were incubated with blocking buffer (1% BSA, 0.1% Triton X-100, 20% serum in PBS) for 1 h at room temperature and then with the following primary antibodies diluted in blocking buffer

for 16 h at 4°C: anti-NeuN 1:300 (MAB377, Millipore Bioscience Research Reagents), anti-GFAP 1:1000 (N1506, Dako), anti-Olig-2 1:200 (Q13516, Millipore Bioscience Research Reagents) and anti-Cd11b 1:100 (MCA74G, Serotec). Slices were washed 3 times with PBS for 10 min each and incubated with secondary antibody 1:600 prepared in blocking buffer, for 2 h at room temperature: anti-Rabbit Alexa 488, anti-Mouse Alexa 594, anti-Rat Alexa 488, or anti-Rabbit Alexa 594. The slices were then washed 3 times for 10 min each with PBS and mounted using Fluoromount and Hoechst 1:5000 with a coverslip. Coverslips were sealed with nail polish and stored at 4°C protected from light. Tissue sections were viewed with an Olympus IX71 microscope and images were captured using a QImaging QICAM Fast 1394 camera. Numbers of motoneurons were assessed by counting NeuN-positive cells with motoneuron morphology in the ventral horn of the spinal tissue.

6.4.3. Immunohistochemistry analysis.

Brain slices were washed 3 times per 10 min each with PBS and incubated with 0.3% H_2O_2 for 30 min, then washed 2 times per 10 minutes with PBS, incubated with blocking buffer (0.5% BSA, 0.2% Triton X-100, 0.02% sodium azide in 1X PBS) for 1 h at room temperature followed by incubation with anti-calbindin 1:200 (C26D12, Cell Signaling) primary antibody prepared in blocking buffer for 16 h at 4°C. Slices were washed 4 times for 10 min each with PBS and incubated with secondary antibody rabbit IgG (Vectastain).prepared in 0.5% BSA and 0.2% Triton X-100 at a dilution of 1:500 for 2 h at room temperature. After 4 washes with PBS for 10 min each slices were incubated for 1 h at room temperature with 1:1000 reagent A and 1:1000 reagent B (Vectastain) and washed 4 times with PBS for 10 min each, developed with 10 mg DAB (D5905, Sigma Chemical Company), and again washed 3 times with PBS for 10 min each . Finally slices were mounted onto a VWR Micro Slides Superfrost Plus glass (VWR International) with Entellan (Merk) using a coverslip and nail polish to seal it. Tissue sections were viewed

with a Nikon Eclipse 80*i* microscope and images were captured using a Nikon DS-*Fi*1 camera. The number of cerebellar crests, maximum layers of PC and number of cells were counted.

6.5. SDS-PAGE and Western blot analysis of cell cultures and tissue extracts.

For tissue samples, pieces with a five mm diameter of cerebellum, cortex, hippocampus and liver were collected and homogenized in 1X RIPA buffer (50mM Tris, 150 mM NaCl, 1% Triton X-100, 0.5% deoxycholate, 0.1% SDS with protease inhibitor cocktail (PIC, Roche)). For cell culture samples cells were lysed using a 1X NP40 buffer (1% NP40, 150 mM NaCl, 50 mM Tris pH 8.5 with protease inhibitor cocktail). The extracts were sonicated 3 times for 5 sec and the protein concentration was determined using the BCA Protein Assay Kit (Pierce).

Protein samples were prepared using 10-75 µg of total proteins incubated with 100 mM DTT for 10 min at room temperature, then mixed with 5X sample buffer (0.2 M Tris-HCl pH 6.8, 10% SDS, 0.05% Bromphenolblue, 20% glycerol) and cooked for 5 min at 95°C.

The 8% polyacrylamide separation gel was prepared with 380 mM Tris-HCl pH 8.3, 8% acrylamide-bis-acrylamide, 0.1% SDS, 0.1% ammonium persulfate and 0.06% TEMED. The 4% polyacrylamide stacking gel were prepared with 60 mM Tris-HCl pH 6.8, 4% acrylamide-bis-acrylamide, 0.1% SDS, 0.1% ammonium persulfate and 0.06% TEMED. Electrophoresis was run in running buffer (25 mM Tris, 250 mM glycine and 0.1% SDS) at a constant voltage of 60 V until the front entered the separation gel at which point the voltage was adjusted to 100 V. The run was stopped when the blue front left the gel.

Proteins were transferred to a PVDF membrane in transfer buffer (25 mM Tris, 250 mM glycine and 20% methanol) at a constant voltage of 120 V for 2 h on ice. The membranes were then incubated with a blocking buffer (5% milk in PBS) for 1 h at room

temperature. After 3 washes 10 min each with PBS containing 0.1% Tween-20 (wash buffer) membranes were incubated with either of the following antibodies diluted in blocking buffer: anti-ERp57 1:3000 (SC-28823, Santa Cruz), anti-HSP90 1:3000 (SC-7947, H114, Santa Cruz), anti-PDI 1:3000 (SPA-891, ENZO/Stressgen), anti-ERp72 1:3000 (SPS-720, ENZO/Stressgen), anti-ERO1 1:3000 (NB-100-2525, Novus Biologicals), anti-calnexin 1:3000 (SPA-865, ENZO/Stressgen), anti-BIP 1:1000 (SPA-826, ENZO/Stressgen), anti- βactin HRP-conjugate 1:1000 (5125, Cell Signaling) overnight (~16 h) at 4°C. The membranes were washed 3 times with wash buffer 10 min each and incubated with secondary antibody anti-mouse-HRP or anti-rabbit-HRP (both Invitrogen) diluted 1:3000 in blocking buffer. Again membranes were washed with wash buffer 3 times for 10 min each and developed using the ECL Western Blotting Substrate kit (Pierce) and Super HR-U photographic films (Fujifilm). To quantify the protein levels obtained, the intensity of the bands were calculated using ImageJ software and the values were normalized to the intensity obtained for HSP90 or actin as a loading control and to the values obtained for wildtype lanes.

6.6. RNA extraction and RT-PCR.

Total RNA was prepared from cortex, cerebellum and hippocampus tissue previously homogenized in PBS using TRIzol (Invitrogen). cDNA was synthesized by iScript cDNA Synthesis kit (BioRad) using 2 µg of RNA, 10X RT buffer, 1 mM dNTPs each one, 10X random primers p(dN)6 (Roche, Basel, Switzerland) and 1 µL of reverse transcriptase in a final volume of 20 µL, using the program: 5 min at 25°C, 45 min at 44°C and 5 min at 85°C.

Quantitative real-time PCR was performed employing SYBR green fluorescent reagent in a mix that contained 4 µL of a 1:40 dilution of cDNA, 10X buffer SYBR Mix, 0.16 mM of each dNTP , 100X SYBR green, 0.1 µM of each primer and 0.25 µL of Go Taq Flexi enzyme (Promega) in a final volume of 25 µL. The following primers were used:

erp57 forward 5'-GAGGCTTGCCCCTGAGTATG -3'

erp57 reverse 5'-GTTGGCAGTGCAATCCACC -3'

actin forward 5'-CTCAGGAGGAGCAATGATCTTGAT-3'

actin reverse 5'-TACCACCATGTACCCAGGCA-3'

The qPCR program used was: 10 min at 95°C (denaturation cycle), 35 cycles of 15 sec at 95°C, 15 sec at 57°C, 15 sec at 72°C and one cycle of 10 sec at 95°C, 5 sec at 25°C, 1 sec at 70°C and 1 sec at 95°C in an ABI PRISM7700 system (Applied Biosystems). The summary of the experiments done in the *erp57* knockout mice is shown in the Figure 7, with the progression of the age of the mice.

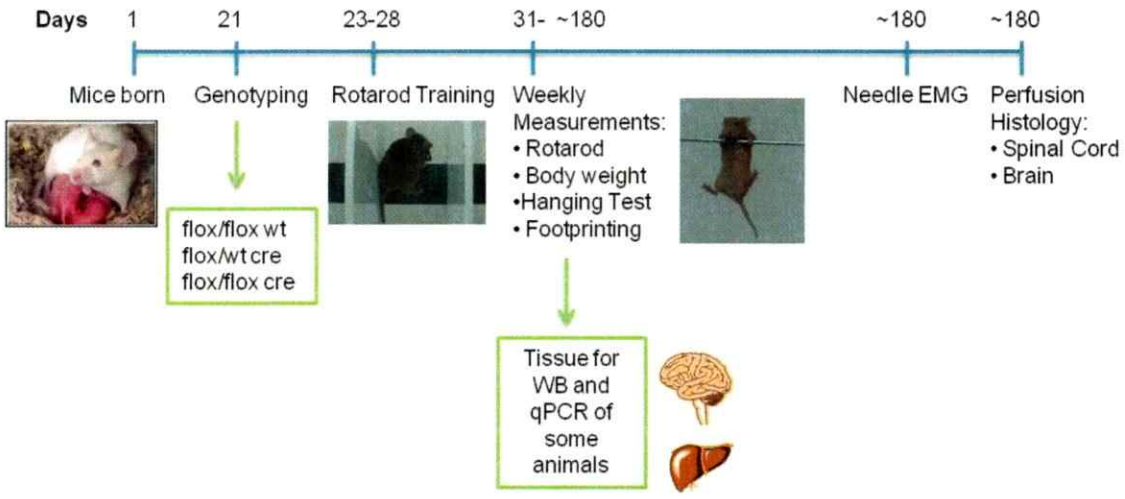

Figure 7. Time-course of the experiments performed in *erp57* knockout mice. Started in the birth of the mouse, at 21 days the mice were weaned and the genotyping was done. Once known genotype, the mice selected were the wildtype (flox/flox wt), heterozygous (flox/wt cre) and knockout (flox/flox cre) for the rotarod training for 5 consecutive days. After finish this, the body weight measurements were done with the rotarod, hanging test and footprinting until 6 months of age approximately. Some mice were used for extract tissue for Western blot and qPCR analysis: cortex, cerebellum, hippocampus and liver as a control. Then, the mice were subjected to an electromyogram (Needle EMG) and a perfusion to obtain the spinal cord and the brain for histological analysis.

6.7. Generation of a CNS ERp57 transgenic mouse model.

The expression plasmid MoPrP.XhoI was kindly provided by David Borchelt of the Johns Hopkins School of Medicine, Baltimore, USA (Borchelt et al., 1996). In our laboratory the human ERp57 gene (Gene ID: 2923) derived from cDNA was introduced into the plasmid together with the sequence coding for a flag tag using the XhoI restriction site. The resulting plasmid expresses the ERp57 gene fused to a Flag tag under the control of the PrP promoter (Figure 8A) and was sent to the "Centro de Estudios Científicos" (CECS), Valdivia, to generate ERp57 transgenic mice. The plasmid was purified, prepared and linearized for microinjection, performed by trained personal in a designated area of the animal facility. An ovule was extracted from a female mouse after a treatment with 50 IU/mL of Pregnant Mare Serum Gonadotrophin (PMSG) and 0.1 mL of 50 IU/mL human Chorionic Gonadotrphin (hCG) injected intraperitoneally. Females were breed with males and the zygotes were extracted. The microinjection was done in the male pronucleus of the zygotes and transferred to a pseudo-pregnant female (females crossed with vasectomized males) with approximately 10 to 15 embryos per oviduct (Figure 8B). After 21 days, pups were born and were genotyped to determine the number of transgenic animals. Each obtained transgenic animal will be one independent mouse line with a mixed background C57BL/6. For genotyping DNA was extracted from the tail of the mouse like previously described followed by Touch Down PCR. 1 µL of DNA was incubated with 10 µL of Go Taq Master Mix (Promega) and 1 µM of each primer in a final volume of 20 µL. The primers used were: *erp57* 866 forward 5'-AATTCCTGGATGCTGGGCACAAAC -3' and *erp57* 1535 reverse 5'-TCTGCTTGTCATCGTCGTCCTTGT -3'. The PCR program used was one cycle of denaturation for 5 min at 94°C, 20 cycles of 30 sec at 94°C, 30 sec at 65°C (decreasing 0.5°C per cycle), 50 sec at 72°C; 16 cycles of 50 sec at 94°C, 30 sec at 55°C, 50 sec at 72°C and a final cycle of elongation for 5 min at 72°C. PCR products

were analyzed by agarose gel electrophoresis using 1% agarose gels with 1 µg/mL ethidium bromide and run at 100 V.

Selected transgenic mouse lines were maintained in the facilities of the University of Chile (Santiago, Chile). All experiments and animal care follows the Institutional Review Board´s Animal Care of the University of Chile (CBA # 0305 FMUCH).

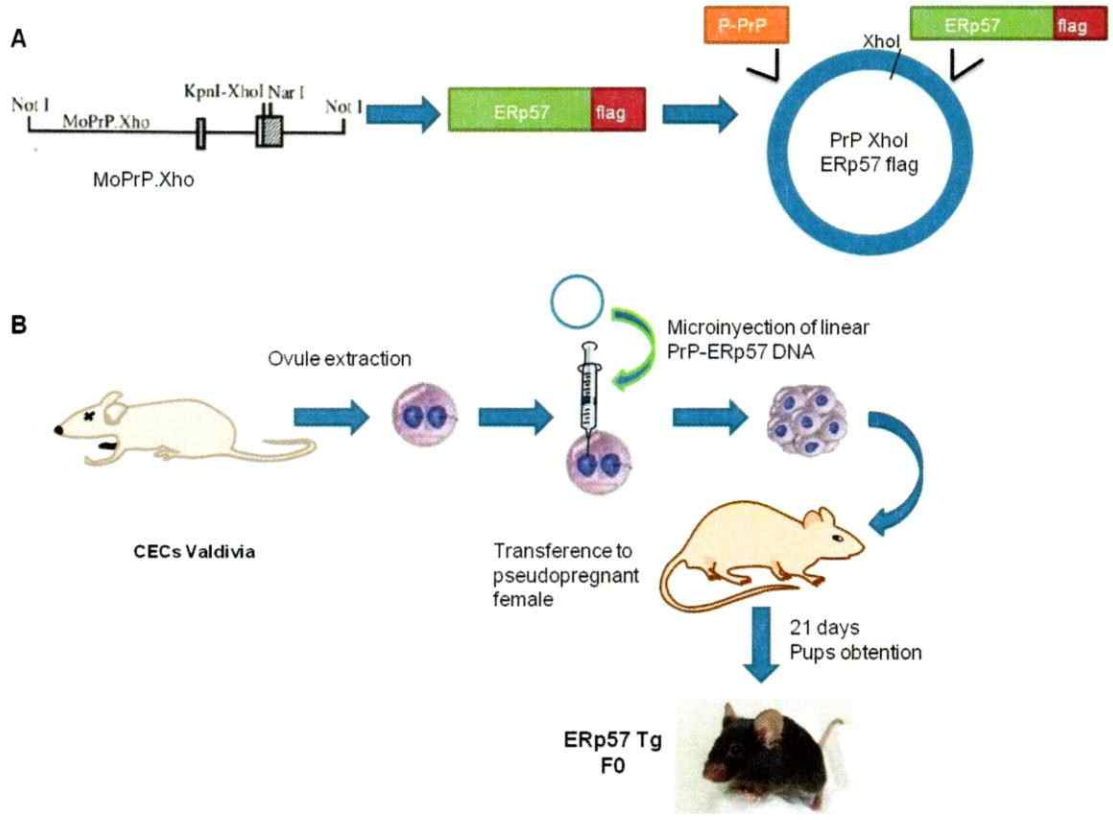

Figure 8. Strategy used to generate an ERp57 transgenic mice. (A) Cloning previously done in the laboratory for generate the plasmid containing the human ERp57 gene with the Flag tag under the control of the prion promoter using the expression plasmid MoPrP.XhoI and the XhoI restriction site. (B) In the CECs, Valdivia, the transgenic mouse was generated. For that, a microinyection of the plasmid obtained in (A) was done in a zygote extracted from a female mouse and transferred to a pseudopregnant female. After 21 days the mice borned and some of the pups were transgenic for ERp57-Flag. These transgenic animals were the F0 and each one constituted an independent line.

6.8. Statistical analysis.

Data are shown as mean +/- SEM. Statistical analyses were performed using Student's t-test two-tailed or two-way repeated-measures ANOVA followed by a *Bonferroni´s post hoc* test for multiple comparisons, a P value of <0.05 was considered a statistically significant difference. All statistical analyses were performed using GraphPad Prism 5 software.

7. RESULTS.

7.1. Generation of a conditional *erp57* knockout mouse model.

In order to produce an ERp57 knockout mouse model with specific deletion of ERp57 in the CNS, mice with loxP site flanked *erp57* gene were crossed with mice expressing cre recombinase under the control of the nestin promoter, which is active during the development of neuronal precursors (Mignone et al., 2004). In the resulting mice *erp57* is deleted in tissue derived from neuronal precursors, such as the brain and all CNS. The results of the breedings are described in Material and Methods section 6.1, and Figure 9A.

For genotyping, primers amplifying *erp57* floxed fragment (outlined in Material and Methods section 6.1) were used to detect the floxed allele (387 bp product) in the homozygote and the wildtype allele (200 bp product) with the floxed allele in heterozygote mice (Figure 9B upper panel). The primers used to amplify cre forward and cre reverse were used to show the presence of the cre (100 bp product) (Figure 9B bottom panel). Primers to amplify IL-2 were used as a control.

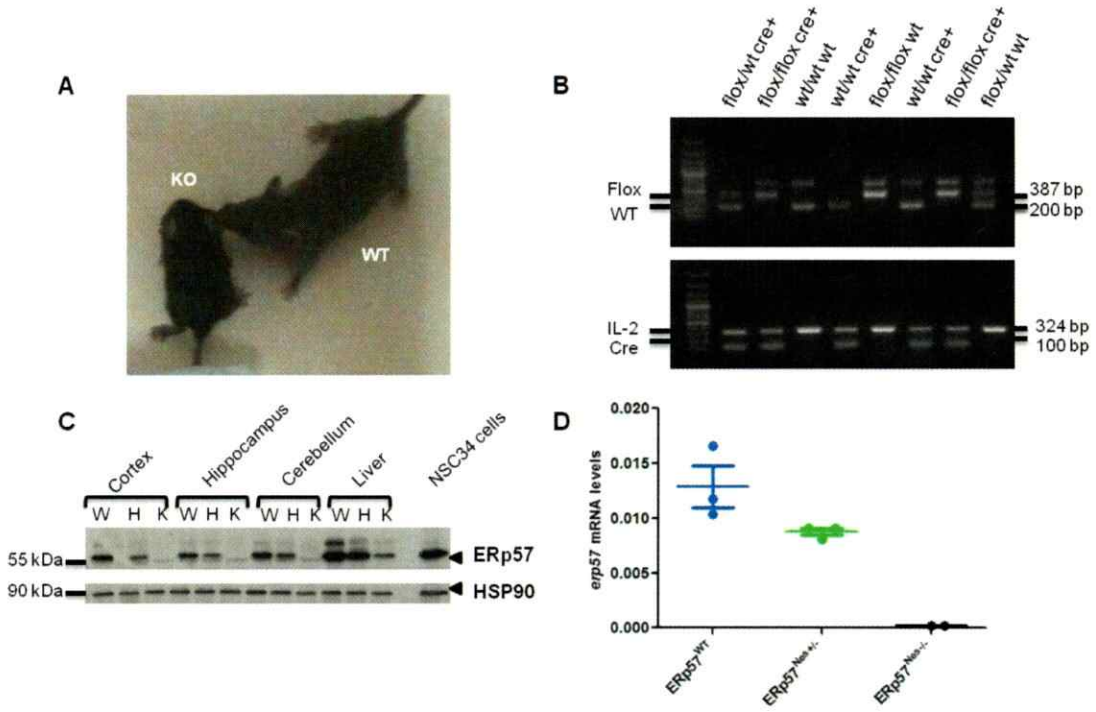

Figure 9. Generation and confirmation of *erp57* knockout mice. (A) Photography of an ERp57$^{Nes-/-}$ mouse (KO) with an ERp57^{WT} littermate (WT). (B) PCR analysis of genomic DNA isolated from ERp57^{WT} (wt/wt wt, wt/wt cre, flox/wt wt, flox/flox wt), ERp57$^{Nes+/-}$ (flox/wt cre) and ERp57$^{Nes-/-}$ (flox/flox cre) mice. Primers *erp57* floxed forward and reverse were used to obtain a 387 bp or 200 bp product in the case of the floxed or wildtype *erp57* allele respectively and gave an unspecific 800 bp approximately higher band (upper panel). The presence of both floxed and wildtype band identifies ERp57$^{Nes+/-}$ mice and only the floxed band identifies the ERp57$^{Nes-/-}$. Cre forward and reverse primers were used to obtain a 100 bp product to demonstrate the presence of the cre recombinase sequence or no product in the case of the absence of the cre sequence (wildtype). The amplification of IL-2 was used as a control (bottom panel). (C) Western blot analysis of ERp57^{WT} (W), ERp57$^{Nes+/-}$ (H) and ERp57$^{Nes-/-}$ (K) tissues with anti-ERp57 antibody. HSP90 was used as a loading control and a protein extract of the motoneuron cell line NSC34 as a control to identify the correct band. (D) *erp57* mRNA levels from cortex were quantified relative to *actin* mRNA levels by real time PCR and mean ± SEM of n=3 for ERp57^{WT}, n=3 ERp57$^{Nes+/-}$ and n=2 animals for ERp57$^{Nes-/-}$. ERp57$^{Nes+/-}$ and ERp57$^{Nes-/-}$ mice showed an *erp57* deletion confirmed by analysis of the protein levels (C) or mRNA levels (D) of brain tissues.

After obtaining a sufficient number of litters of each breeding, the rate of birth was calculated (Table 2). Consistently conditional *erp57* knockout mice were generated in a lower percentage from the expected ratio, whereas heterozygote mice (breeding of an $ERp57^{Nes+/-}$ with an $ERp57^{WT}$) had an increased observed percentage than the expected. In summary, *erp57* knockout mice showed a reduced rate of birth suggesting developmental alterations.

Table 2. Rate of birth in the conditional *erp57* knockout mouse model. The rate of birth was calculated for each breeding. Genotypes of all pups analyzed were determined and are presented as observed number or percentages together with expected percentages. A decrease in the rate of birth was obtained compared with the expected in $ERp57^{Nes-/-}$ mice.

Crossings		Pups			
		$ERp57^{WT}$	$ERp57^{Nes+/-}$	$ERp57^{Nes-/-}$	Total
flox/wt cre X flox/wt wt	Observed No.	41	8	3	52
	Observed %	78.9	15.4	5.7	100
	Expected %	62.5	25	12.5	100
		$ERp57^{WT}$	$ERp57^{Nes+/-}$	$ERp57^{Nes-/-}$	Total
flox/wt cre X flox/flox wt	Observed No.	10	10	3	23
	Observed %	43.5	43.5	13	100
	Expected %	50	25	25	100
		$ERp57^{WT}$	$ERp57^{Nes+/-}$	$ERp57^{Nes-/-}$	Total
flox/flox cre X flox/flox wt	Observed No.	2		1	3
	Observed %	66.7		33.3	100
	Expected %	50		50	100

To confirm the functional deletion of ERp57 in the nervous system compared to other tissues, a Western blot was performed with protein extracts from cortex, hippocampus, cerebellum and liver of $ERp57^{Nes-/-}$, $ERp57^{Nes+/-}$ and $ERp57^{WT}$ mice (Figure 9C) using anti-ERp57 antibody. A protein extract of the motoneuron cell line NSC34 was

used as a positive control to identify the correct ERp57 band. As a loading control HSP90 was detected. In brain tissues of ERp57$^{Nes-/-}$ a full reduction in ERp57 levels was obtained (Figure 9C). In addition ERp57$^{Nes+/-}$ mice showed a significant reduction in ERp57 levels. Surprisingly reduced ERp57 levels were also observed in the liver, although in a lesser extent (Figure 9C). The intensity of bands corresponding to ERp57 was semi-quantified with the ImageJ software, normalized to HSP90 values and expressed as percentages relative to the ERp57^{WT} of each tissue (Table 3). In average, the percentage of ERp57 levels in brain tissues derived from ERp57$^{Nes+/-}$ mice was 57% and 2% from ERp57$^{Nes-/-}$ mice compared to the levels observed in ERp57^{WT} mice.

Table 3. Semi-quantitative values of the Western blot analysis of brain tissues and liver tissue from ERp57^{WT}, ERp57$^{Nes+/-}$ and ERp57$^{Nes-/-}$ mice. The values normalized to the HSP90 loading control and each ERp57^{WT} tissue are shown. A reduction in the expression of ERp57 is observed in ERp57$^{Nes+/-}$ and ERp57$^{Nes-/-}$ mice compared to ERp57^{WT} mice in all brain tissues. WT: ERp57^{WT}, HET: ERp57$^{Nes+/-}$, KO: ERp57$^{Nes-/-}$.

Tissue	Genotype	% of WT control
Cortex	WT	100
Cortex	HET	36.2
Cortex	KO	1.7
Hippocampus	WT	100.0
Hippocampus	HET	54.0
Hippocampus	KO	0.6
Cerebellum	WT	100.0
Cerebellum	HET	80.4
Cerebellum	KO	2.4
Liver	WT	100.0
Liver	HET	138.5
Liver	KO	60.6

Due to deletion of the *erp57* gene a reduction of *erp57* mRNA is expected. To confirm the loss of *erp57* mRNA a RT-PCR with specific primers for ERp57 that do not amplify the deleted allele, was performed. RNA was extracted from the cortex of ERp57^{WT},

ERp57$^{Nes+/-}$ and ERp57$^{Nes-/-}$ mice and the cDNA was prepared. The levels of *erp57* mRNA were normalized to the *actin* mRNA levels as shown in the Figure 9D. The *erp57* deletion was confirmed by the complete loss of the *erp57* mRNA in ERp57$^{Nes-/-}$ mice and a partial reduction in ERp57$^{Nes+/-}$ mice compared to ERp57^{WT} animals. Together, these results demonstrate the generation of an *erp57* conditional knockout mouse model for the CNS.

7.2. Analysis of motor functions in *erp57* knockout mice.

To phenotypically analyze the effects caused by *erp57* deletion, ERp57$^{Nes-/-}$ and ERp57$^{Nes+/-}$ mice were characterized by visual observation, body weight measurements, Rotarod test, Hanging test and Footprinting analysis and compared to their ERp57^{WT} littermates.

After visual observation we noticed that the ERp57$^{Nes-/-}$ pups were clearly smaller than their ERp57^{WT} littermates (evident in the Figure 9A). ERp57$^{Nes+/-}$ mice displayed an intermediate size. Another characteristic of ERp57$^{Nes-/-}$ mice was an abnormal movement with a certain degree of difficulty. This observation was more evident up to 2 months of age approximately, and then became less noticeable when the mouse reached 4 months approximately. Also, when mice were held from the tail, ERp57$^{Nes-/-}$ mice did not clasp their legs. Based on these quantitative observations, the reduction in body size was quantified by body weight measurements and the motor phenotype was also assessed by the Rotarod, Hanging test and Footprinting assay.

The body weight was measured every week in ERp57^{WT} mice, ERp57$^{Nes+/-}$ mice and ERp57$^{Nes-/-}$ mice starting from 31 days of age until 150 days of age (Figure 10). ERp57$^{Nes-/-}$ mice displayed a 40% reduction of body weight during the complete duration of measurements. ERp57$^{Nes+/-}$ mice also presented a decrease in the body weight, although to a lesser extend as observed for ERp57$^{Nes-/-}$ mice (Figure 10). Although differences were greater during a younger age, still the differences were maintained over time.

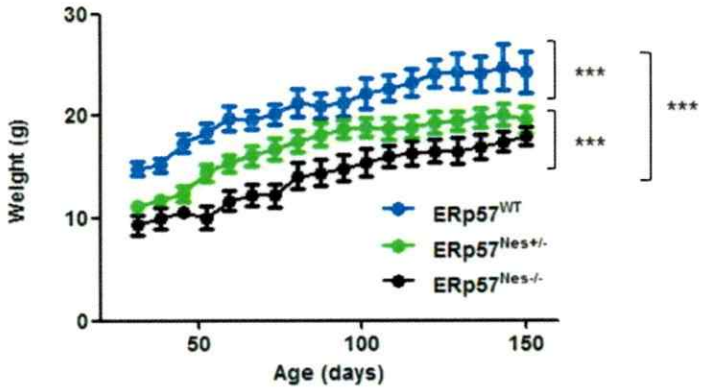

Figure 10. Body weight gain progression of ERp57^{WT}, ERp57$^{Nes+/-}$ and ERp57$^{Nes-/-}$ mice. Body weight measurements started at 31 days of age until 150 days of age once per week with a maximum of n=18 ERp57^{WT}, n=7 ERp57$^{Nes+/-}$ and n=9 ERp57$^{Nes-/-}$ mice. Mean ± SEM of each group are shown. ERp57$^{Nes-/-}$ and ERp57$^{Nes+/-}$ mice (black and green curves respectively) showed a considerable reduction of body weight compared to ERp57^{WT} mice (blue curve). ERp57$^{Nes+/-}$ mice exhibited an intermediate body weight between ERp57^{WT} and ERp57$^{Nes-/-}$ mice. *P* values are shown: ***, $p<0.001$; Two-way ANOVA and *Bonferroni´s post hoc* test.

Rotarod tests were performed every week starting from 38 days of age until 129 days of age. The time until the mouse fell from the rod was measured with a maximum of 120 seconds and is shown in Figure 11. Although considerable variability of values was obtained, a clear tendency was observed. ERp57$^{Nes-/-}$ mice consistently performed worst in the Rotarod (the reduction in the time compared to ERp57^{WT} was near to 80%) with a significant difference compared to ERp57^{WT} and ERp57$^{Nes+/-}$ mice. ERp57$^{Nes+/-}$ animals performed better than ERp57$^{Nes-/-}$ mice, sometimes similar but in general with intermediate conduct and with no significant difference compared to ERp57^{WT} (Figure 11). In the Rotarod test no obvious progression of phenotype in time was observed.

For the Hanging test, the mouse was placed to hang on a horizontal bar and a score was assigned based on the reaction of the mouse within 30 seconds. This test was performed once per week, 3 times in one day. The scores obtained are shown in Figure 12. ERp57$^{Nes-/-}$ mice obtained the lower score (in average 1), whereas ERp57$^{Nes+/-}$ performed comparably well with a score of 4 and ERp57^{WT} mice obtained the maximum score of 5. The differences obtained in this test, which measures coordination and motor

skills were greater compared to other tests performed. In some cases, ERp57$^{Nes-/-}$ mice were even not able to support themselves on the bar.

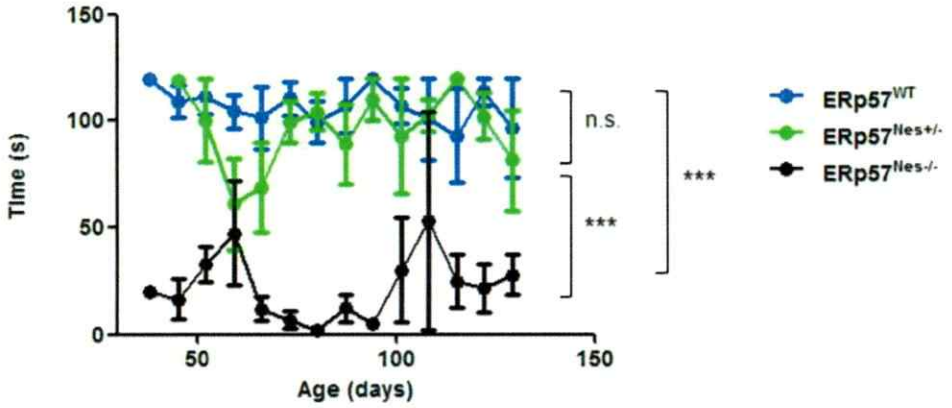

Figure 11. Rotarod performance of ERp57^{WT}, ERp57$^{Nes+/-}$ and ERp57$^{Nes-/-}$ mice. Rotarod test was performed every week, the time until the mouse fell from the rod was recorded with a maximum of 120 seconds. The measurements started at 38 days of age until 129 days of age with a maximum of n=14 ERp57^{WT}, n=6 ERp57$^{Nes+/-}$ and n=9 ERp57$^{Nes-/-}$ mice. Mean ± SEM of each group are shown. ERp57$^{Nes-/-}$ mice (black curve) exhibited a worst performance compared to ERp57^{WT} mice (blue curve) and ERp57$^{Nes+/-}$ (green curve) showed intermediate times, similar to ERp57^{WT} mice in some time points. *P* values are shown: n.s., non significant, $p>0.05$; ***, $p<0.001$; Two-way ANOVA and *Bonferroni´s post hoc* test.

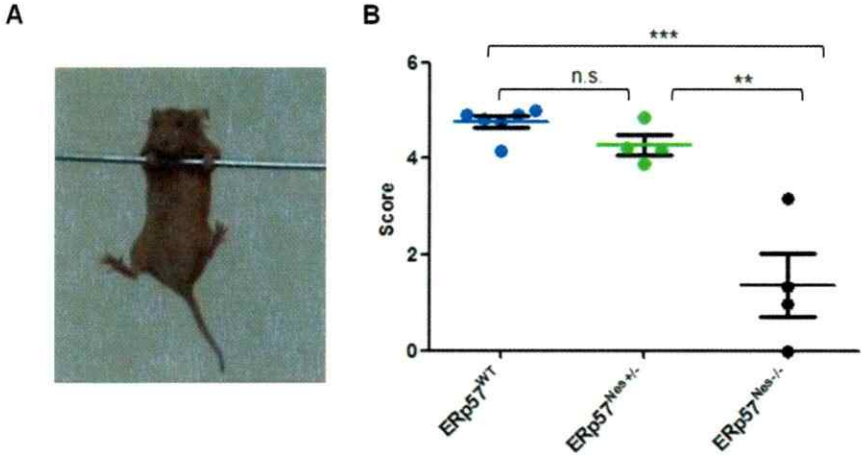

Figure 12. Hanging test scores of ERp57^{WT}, ERp57$^{Nes+/-}$ and ERp57$^{Nes-/-}$ mice. (A) Hanging test was performed every week; the mouse was placed to hang on a horizontal bar. The reaction of the mouse was recorded for 30 seconds. (B) A score was assigned depending on how and if the mouse attempted to escape the bar in the given time. A score maximum of 5 can be reached. Mean ± SEM was plotted with n=6 ERp57^{WT}, n=4 ERp57$^{Nes+/-}$ and n=4 ERp57$^{Nes-/-}$ mice. ERp57$^{Nes-/-}$ mice (black points) exhibited the lowest scores compared to ERp57^{WT} (blue points) and ERp57$^{Nes+/-}$ (green points) mice that achieved scores near to the maximum. *P* values are shown: n.s., $p>0.05$; **, $p<0.01$; ***, $p<0.001$; Student's *t*-test.

Additionally, the Footprinting test was performed. The forelimbs and hindlimbs of mice were painted with nontoxic dyes red and black respectively and the mice were placed to run in a tunnel with white paper at the bottom to obtain the footprint of the each paw. Visually it was difficult to see a difference since the footprints obtained from $ERp57^{Nes-/-}$ and $ERp57^{Nes+/-}$ mice where overall similar to $ERp57^{WT}$ (Figure 13A). However, a slight difference in the path of movement was observed, which for some $ERp57^{Nes-/-}$ mice was more disordered compared to $ERp57^{WT}$.

Measurements of the steps and the footprint were made in at least six steps of each Footprinting test performed. The angle of rotation was evaluated as the angle made by two lines that connect the third toe with a line at the center of the hindlimb paw. The result is shown in Figure 13B, in this measure no significant difference was found between $ERp57^{Nes-/-}$ and $ERp57^{WT}$ mice. The interlimb coordination was described as the distance between the center of the pad of forelimb and the ipsilateral hindlimb and is shown in Figure 13C, which exhibits a slight increase in the values obtained for $ERp57^{Nes+/-}$ and $ERp57^{Nes-/-}$ mice compared to $ERp57^{WT}$ mice, but the difference was not significant. Finally, the distance between limbs was measured as the distance from one hindlimb to the next one and the result obtained is presented in Figure 13D. $ERp57^{Nes+/-}$ mice showed an increase in the distance, different from $ERp57^{Nes-/-}$ mice that exhibited a slight decrease compared to $ERp57^{WT}$ mice, and again this difference was not significant.

In summary, the test performed revealed a motor impairment caused by the deletion or reduction of *erp57* in the CNS.

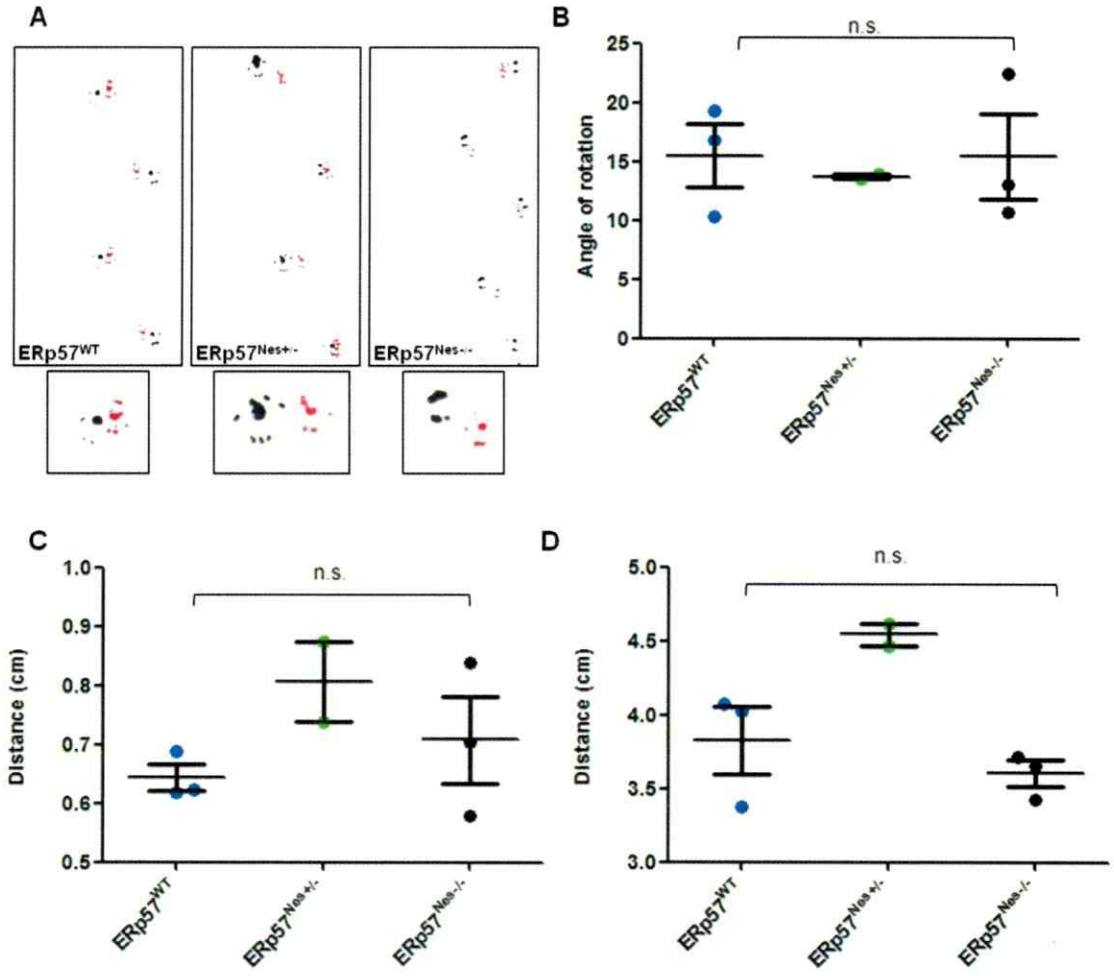

Figure 13. Footprinting images of ERp57^{WT}, ERp57$^{Nes+/-}$ and ERp57$^{Nes-/-}$ mice. (A) Footprinting analysis was performed every week. The forelimbs and hindlimbs of the mouse were painted with nontoxic dyes red and black, respectively. Then the mouse was placed to run in a narrow tunnel with white paper at the bottom. A representative footprinting image of ERp57^{WT}, ERp57$^{Nes+/-}$ and ERp57$^{Nes-/-}$ mice is shown with a zoom of one footprint. n=3 ERp57^{WT}, n=2 ERp57$^{Nes+/-}$ and n=3 ERp57$^{Nes-/-}$ mice, with at least 4 prints per mouse. (B) Angle of rotation was measured as the angle made by two lines connecting the third toe and the stride line at the center of the paw pad in the hindlimb. No significant difference was found by genotype. (C) Interlimb coordination was measured as the distance between the center pads of the ipsilateral forelimb and hindlimb. There was a slight increase in the interlimb coordination in ERp57$^{Nes-/-}$ and ERp57$^{Nes+/-}$ compared to ERp57^{WT}, but nothing significant. (D) Distance between limbs was recorded as the distance from one hindlimb to the next one. ERp57$^{Nes-/-}$ mice showed a decrease in the distance between limbs compared to ERp57^{WT} and ERp57$^{Nes+/-}$ an increase, but nothing significant. At least six steps were analyzed of each footprinting test for each measurement. The mean ± SEM of the average of each mouse by group is shown. *P* values are shown: n.s., $p>0.05$; Student's *t*-test.

7.3. Muscle innervations in *erp57* conditional knockout mice.

In order to investigate if the motor impairment observed in ERp57$^{Nes-/-}$ mice was due to a muscle problem, a Needle Electromyogram (EMG) was performed. To measure the muscular activity, the mouse was anesthesized and a needle electrode was introduced consequently in the muscles of all four extremities to record the signal. In Figure 14, representative images of the EMG obtained for each genotype are shown. In A, the resulting EMG of an ERp57^{WT} mouse indicates a normal muscle at rest. In B, the EMG obtained for an ERp57$^{Nes+/-}$ mouse displays the presence of Positive Sharp Waves (PSW), a sign of denervation of the muscle (Figure 14). Only in 2 of 5 ERp57$^{Nes+/-}$ animals the presence of PSW was found. In C, the EMG from a ERp57$^{Nes-/-}$ mouse is shown, where the PSW was stronger and was present in all animals investigated, being a sign of more serious denervation of the muscle (Figure 14). SOD1^{G86R} ALS transgenic mice were used as a positive control, in the case of a symptomatic mouse the PSW were easily detected (Table 4). The presence of the PSW was quantified by a score assigned to each measure: 0 is when PSW were absent, +1 when PSW were observed in a minimum of one extremity, +3 when PSW are easily detected immediately when the needle is inserted into the muscle, and +2 in any case intermediate of criteria applied for scores +1 and +3. The scores obtained for each animal group are summarized in Table 4. For ERp57^{WT} mice, all the animals showed a score of 0 because the PSW in the signal was absent. For ERp57$^{Nes+/-}$ 2 of 5 mice the PSW appeared in some of the muscles analyzed, the remaining 3 animals did not present any PSW and were scored a 0. In the ERp57$^{Nes-/-}$ mice, the 3 animals showed a score of +1 because the PSW appeared in some muscles analyzed or in some points of the legs. The pre-symptomatic SOD1^{G86R} transgenic mice displayed a score of 0 however a late-stage symptomatic SOD1^{G86R} transgenic mouse was scored +3 with PSW easily detected in all points of measurement, which served as a positive control of the measurement. These results in conjunction indicate the presence of muscle damage

in the ERp57$^{Nes-/-}$ mice and in some ERp57$^{Nes+/-}$ mice compared to normal muscle phenotype in ERp57^{WT} animals.

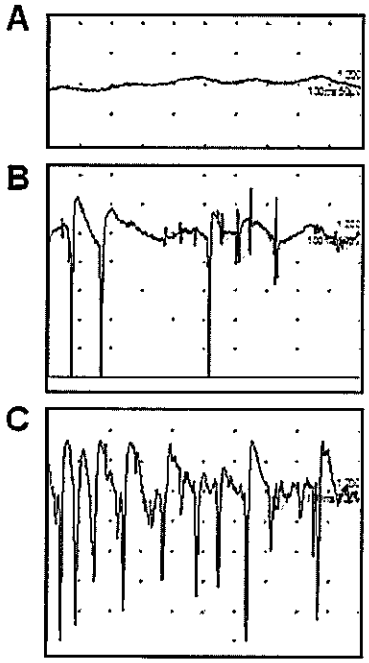

Figure 14. Electromyogram graphs of ERp57^{WT}, ERp57$^{Nes+/-}$ and ERp57$^{Nes-/-}$ mice. At 6 months of age ERp57^{WT}, ERp57$^{Nes+/-}$ and ERp57$^{Nes-/-}$ mice were subjected to a Needle EMG. The curves of voltage measured in time are shown. (A) A representative image for EMG done in ERp57^{WT} mice. (B) A representative image for EMG curves obtained in ERp57$^{Nes+/-}$ mouse. (C) A representative EMG image for an ERp57$^{Nes-/-}$ mouse. The presence of positive sharp waves (PSW) in ERp57$^{Nes+/-}$ and ERp57$^{Nes-/-}$ mice indicated a muscle denervation compared to the curve obtained in ERp57^{WT} mice. n=9 ERp57^{WT}, n=5 ERp57$^{Nes+/-}$ and n=3 ERp57$^{Nes-/-}$ mice.

Table 4. Summary of EMG results for ERp57^{WT}, ERp57$^{Nes+/-}$, ERp57$^{Nes-/-}$ and SOD1^{G86R} transgenic mice. Positive sharp waves (PSW) were measured in muscles of ERp57$^{Nes+/-}$ and ERp57$^{Nes-/-}$ mice. SOD1^{G86R} and ERp57^{WT} mice were used as control. (a): presymptomatic mice, (b): mouse in the end stage of disease.

Genotype	PSW	n
ERp57^{WT}	0	9
ERp57$^{Nes+/-}$	+1/0	2/3
ERp57$^{Nes-/-}$	+1	3
SOD1$^{G86R\ (a)}$	0	4
SOD1$^{G86R\ (b)}$	+3	1

7.4. Histological analysis of spinal cord and brain of *erp57* knockout mice.

In order to study if cellular changes in brain or spinal cord in ERp57$^{Nes-/-}$ mice are responsible for the motor impairment observed, a histological analysis was performed to visualize neurons and glias. ERp57$^{Nes-/-}$ and ERp57^{WT} littermates of aproximatelly 180 days of age were perfused, the brain and the spinal cord was extracted, processed and sliced for histology. For brain histology, immunohistochemistry was performed with anti-calbindin, antibody, a marker for PC in the cerebellum. In Figure 15A, a representative image of the immunohistochemistry of each genotype is shown. The number of lobules of the entire cerebellum, the maximum number of layers of PC and the number of cells was measured and showed in Figure 15B, C and D, respectively; with two slices analyzed per mouse. No changes in cerebellum structure were found in ERp57$^{Nes-/-}$ mice compared to ERp57^{WT} in any of the parameters evaluated.

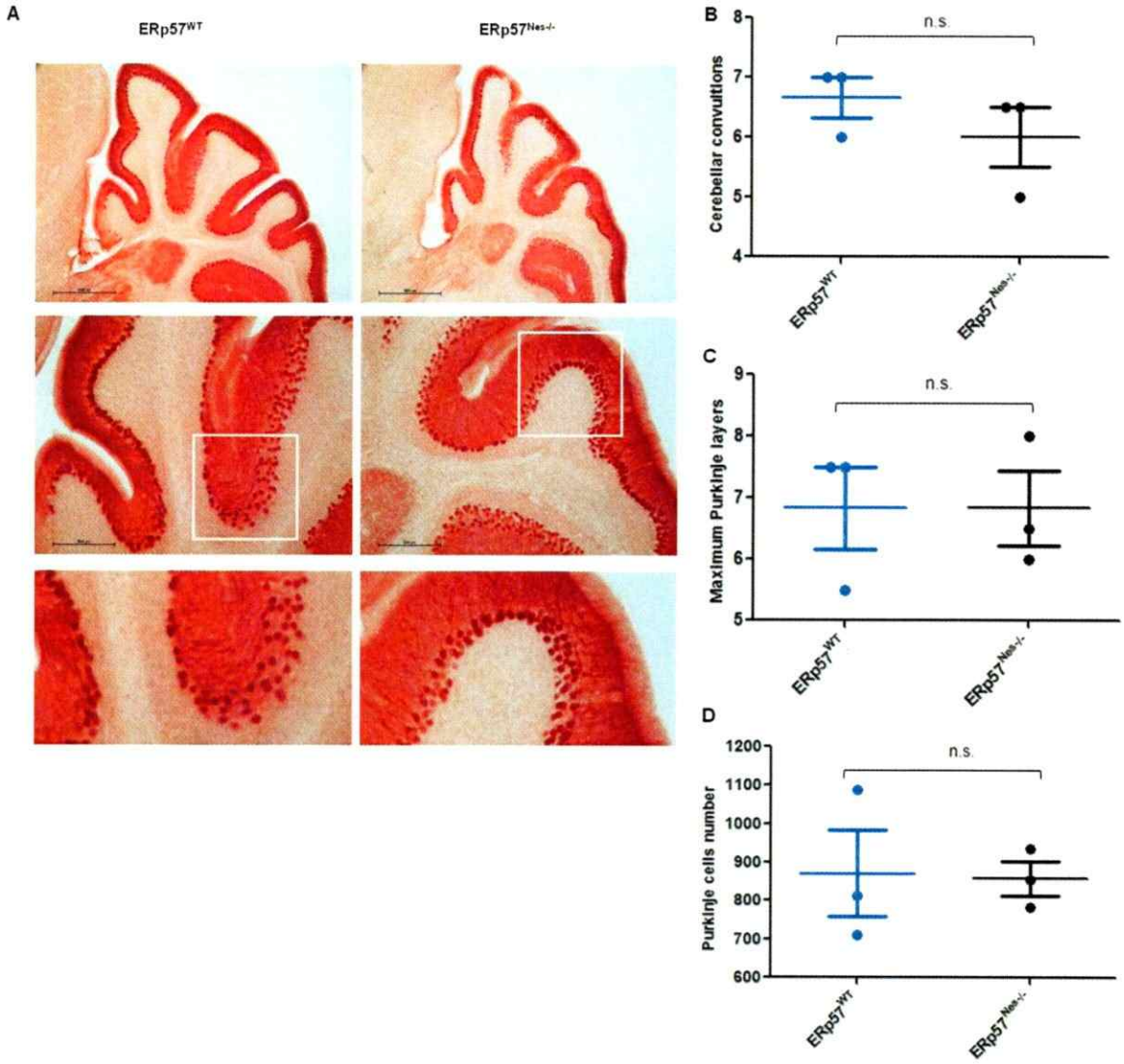

Figure 15. Histological analysis of the cerebellum from ERp57^{WT} and ERp57$^{Nes-/-}$ mice. (A) At 6 months of age, ERp57^{WT} and ERp57$^{Nes-/-}$ mice were perfused and the brain was processed for immunohistochemistry for the PC marker Calbindin. n=3 ERp57^{WT} and n=3 ERp57$^{Nes-/-}$ mice. Scale bars represent 480 µm in the first panels, and 1200 µm in the second panels. (B) Lobules of the cerebellum were quantified. No difference was observed between genotype. (C) The maximum number of PC layers was quantified. No changes were observed by genotype. (D) Number of total PC was quantified. No difference was observed by genotype. In the graphics, mean ± SEM and *P* values are shown: n.s., $p>0.05$; Student's *t*-test.

For spinal cord histology, immunofluorescence was performed with anti-GFAP (a marker of astrocytes) and anti-NeuN (a marker of neurons) antibodies and Hoechst straining for the nucleus. In Figure 16A, a representative image of the immunofluorescence of each genotype is shown: first panel in green is GFAP, second panel in red is NeuN, third panel is the overlay of GFAP, NeuN and Hoechst staining and the fourth panel has a highest magnification.

The number of neurons with the clasical morphology of a motoneuron was assessed using ImageJ as shown in Figure 16B. Three images per mouse were analyzed. The number of NeuN positive particles bigger than a defined size in the ventral horn of the spinal cord caudal zone was quantified. A slight but significant decrease in motoneuron number was found in ERp57$^{Nes-/-}$ mice compared to ERp57^{WT} mice (Figure 16B). The size of motoneurons was also measured (shown in Figure 16C). No differences were observed between motoneurons of ERp57$^{Nes-/-}$ mice compared to ERp57^{WT} mice (Figure 16C). No changes in GFAP staining were detected when ERp57^{WT} and ERp57$^{Nes-/-}$ mice were compared (Figure 16A).

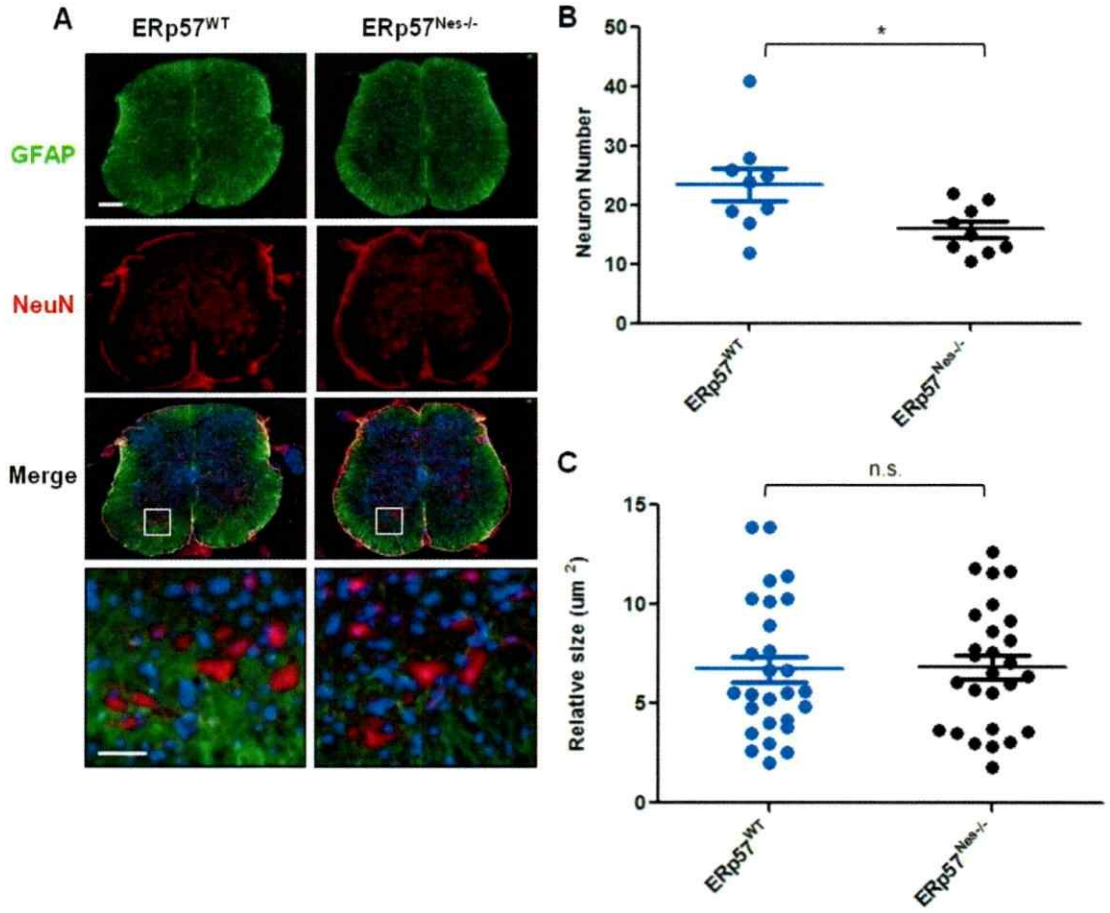

Figure 16. Histological analysis of spinal cord tissue from ERp57^{WT} and ERp57$^{Nes-/-}$ mice. (A) At 6 months of age, ERp57^{WT} and ERp57$^{Nes-/-}$ mice were perfused and spinal cords were processed for immunofluorescence using specific antibodies for GFAP (astrocyte marker) and NeuN (neuron marker). The nucleus was stained with Hoechst. n=3 ERp57^{WT} and n=3 ERp57$^{Nes-/-}$ mice. Scale bars represent 200 µm. (B) Motor neuron numbers in the ventral horn were quantified from 3 images per animal. ERp57$^{Nes-/-}$ mice showed a decreased number of motoneuron in the spinal cord compared to ERp57^{WT} animals. Mean ± SEM of the quantification per group and *P* values are shown: *, $p<0.05$; Student's *t*-test. (C) Relative size of motoneurons analyzed in spinal cord of ERp57^{WT} and ERp57$^{Nes-/-}$ mice. No difference of motoneuron size was observed between the groups. Mean ± SEM and *P* values are shown: n.s., $p>0.05$; Student's *t*-test.

7.5. Protein levels of ER chaperones and PDIs in ERp57$^{Nes-/-}$ mice.

To investigate the underlying molecular mechanism leading to motor impairment observed in ERp57$^{Nes-/-}$ and ERp57$^{Nes+/-}$ mice, the protein levels of other PDI family members, such as PDI and ERp72, as well as ER chaperones CNX and BIP (also called Grp78) were determined. In addition, ERO1 was included in the analysis, since it is an important protein responsible for recycling PDI family member into their active form. Actin was used as a loading control, and liver as a control tissue. The results of the Western blot analysis of brain tissues (cortex, hippocampus, and cerebellum) and liver of individual mice are shown in Figure 17. Semi-quantification with normalization to actin and ERp57^{WT} tissue was also performed (Table 5).

In Figure 17A, Western blot analysis for cortex proteins showed a considerable reduction of CNX, PDI and ERp72 levels in ERp57$^{Nes+/-}$ and ERp57$^{Nes-/-}$ mice. ERO1 and BIP levels were slightly decreased. In hippocampus, increased levels of ERO1, CNX, BIP and PDI in the ERp57$^{Nes+/-}$ and ERp57$^{Nes-/-}$ mice were observed (Figure 17B). The levels of PDI were 3 times increased in the ERp57$^{Nes-/-}$ when compared to ERp57^{WT} (Table 5). ERp72 levels were decreased in the ERp57$^{Nes-/-}$ compared to the same tissue in the ERp57^{WT} and ERp57$^{Nes+/-}$ (Table 5). In cerebellum, decreased levels of PDI, BIP and ERp72 were found (Figure 17C). In ERp57$^{Nes+/-}$ mice, also an increase of BIP and ERO1 levels and an important decrease in PDI levels were detected (Figure 17C). In the liver the pattern of bands for ERO1 and CNX changed completely compared to brain tissues (Figure 17D). A slight increase in the levels of these proteins in the ERp57$^{Nes+/-}$ mice compared to ERp57^{WT} and ERp57$^{Nes-/-}$ mice was observed in liver (Table 5). PDI and BIP were decreased in ERp57$^{Nes-/-}$ and ERp57$^{Nes+/-}$ mice, in addition to ERp72 that was diminished in ERp57$^{Nes-/-}$ mice compared to ERp57^{WT}. Overall, the result of the Western blot analyses demonstrated that the protein levels of many chaperones of the ER and

other PDI family members were altered in ERp57$^{Nes+/-}$ and ERp57$^{Nes-/-}$ mice compared to ERp57^{WT}.

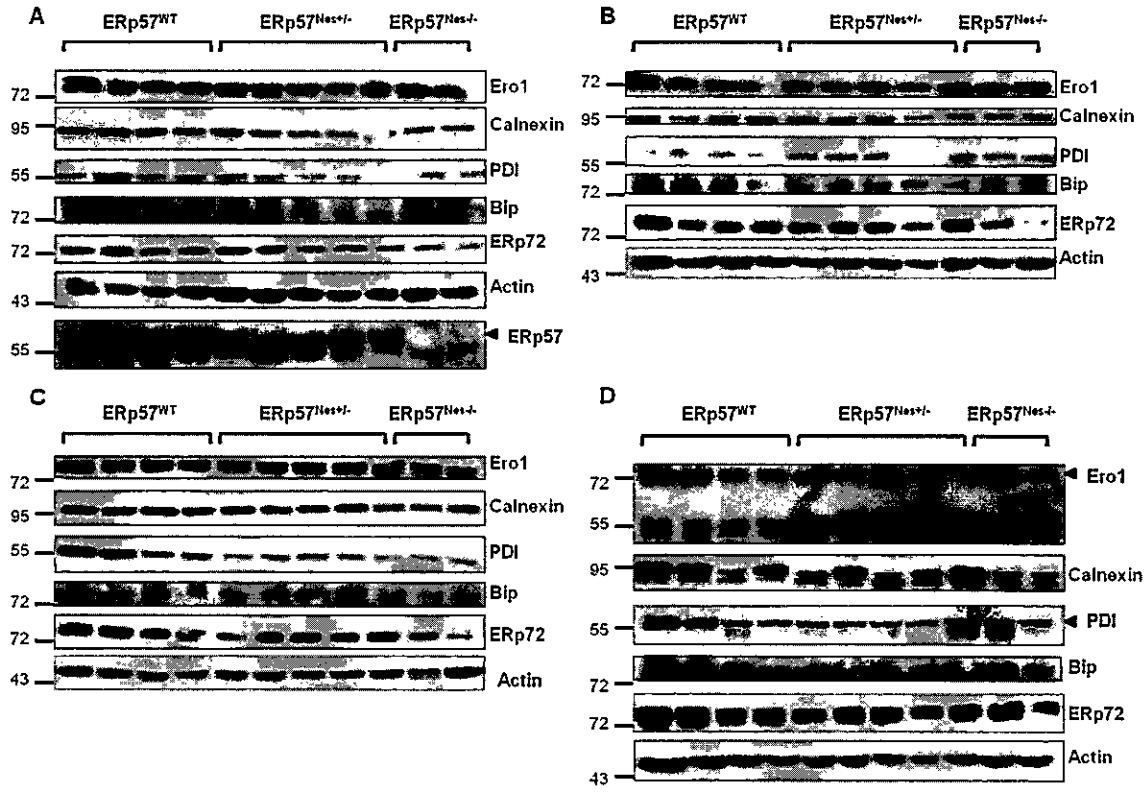

Figure 17. Western blot analysis of brain tissues from ERp57^{WT}, ERp57$^{Nes+/-}$ and ERp57$^{Nes-/-}$ mice. Protein levels of ERO1, CNX, PDI, BIP and ERp72 were analyzed by Western blot using respective antibodies. Actin was used as a loading control. Samples of cortex (A), hippocampus (B), cerebellum (C) and liver (D) of n=4 ERp57^{WT}, n=5 ERp57$^{Nes+/-}$ and n=2 ERp57$^{Nes-/-}$ mice were analyzed. The pattern of the bands observed for ERO1 and CNX in the liver samples was different to the one observed in the brain tissues. A general reduction in the levels of CNX, PDI, ERp72 and BIP was found in ERp57$^{Nes-/-}$ mice. ERO1 showed similar levels in all groups. Protein levels of ERp57 are showed in cortex tissue (A). Arrows indicate corresponding band.

Table 5. Semi-quantification of the Western blot analysis of PDI family members and ER chaperones in brain tissues and liver from ERp57^{WT}, ERp57$^{Nes+/-}$ and ERp57$^{Nes-/-}$ mice. The values normalized to actin loading control and each ERp57^{WT} tissue are shown. WT: ERp57^{WT}, HET: ERp57$^{Nes+/-}$, KO: ERp57$^{Nes-/-}$.

	Cortex			Hippocampus			Cerebellum			Liver		
	WT	HET	KO	WT	HET	KO	WT	HET	KO	WT	HET	KO
ERO1	1	0.8	0.72	1	1.01	1.24	1	1.26	0.77	1	1.84	1.11
Calnexin	1	0.64	0.49	1	0.95	1.23	1	1.06	0.62	1	1.37	1
PDI	1	0.4	0.32	1	2.41	3.27	1	0.48	0.31	1	0.74	0.78
BIP	1	1.003	0.84	1	1.65	1.66	1	1.52	0.4	1	0.74	0.85
ERp72	1	0.65	0.28	1	1.06	0.48	1	0.94	0.43	1	1.01	0.81

7.6. Generation of a CNS ERp57 transgenic mouse model.

A plasmid containing the human *erp57* gene fused to a Flag tag and placed under the control of the PrP promoter was previously generated in our laboratory using a well described vector (Borchelt et al., 1996). This plasmid was used to produce a transgenic mouse model over-expressing the human ERp57 protein in the CNS. ERp57 transgenic mice were generated in the CECS in Valdivia using the protocol shown in Figure 8. Five transgenic lines were obtained and confirmed by genomic PCR: ERp57 L721 (Line 1), ERp57 L825 (Line 2), ERp57 L827 (Line 3), ERp57 L835 (Line 4) and ERp57 L838 (Line 5). At least one mouse of each line was sent to our laboratory to confirm the genotype and the over-expression of the human ERp57 protein in brain extracts.

To genotype these animals, it was necessary to design primers and to develop appropriated PCR programs. The primers designed were termed *erp57* 866 f, a forward primer complementary to the sequence of ERp57 and *erp57* 1535r, a reverse primer complementary to the sequence of the plasmid used. The sequence of the primers and the PCR program are described in Material and Methods, section 6.7. A 650 bp product was obtained in the case of a positive transgenic mouse; no product was obtained in the case of an $ERp57^{Non\text{-}Tg}$ animal (Figure 18A).

To determine the possible over-expression of ERp57 in each transgenic line, and to select one mouse line for further phenotypic characterization, Western blot analysis of cerebellum and spinal cord tissue was performed using an anti-ERp57 antibody. HSP90 was used as a loading control (Figure 18B). Then, using the ImageJ software the intensity of each protein band was semi-quantified and normalized first to the HSP90 values, and then to the intensity of protein bands obtained in $ERp57^{Non\text{-}Tg}$ mice (Table 6). Based on this analysis, lines 1 and 5 were selected for maintenance since they presented the highest

over-expression levels (Table 6), reaching almost twice the levels of ERp57 in ERp57^{Non-Tg} mice. Further tissues were analyzed in these two lines: cortex and liver (Figure 18C). In cortex, the over-expression was also observed, but not in the liver, as expected (Figure 18C). Based on this analysis, two female and two male animals of line 1 and one female of line 5 were sent from Valdivia as founders (F0) to expand each colony. Another confirmatory Western blot analysis was performed of the F1 generation derived from these animals (Figure 18D). Cortex and spinal cord tissues were analyzed to confirm that the over-expression of the transgene was maintained over time. After verifying the maintenance of transgene expression in F1, a mouse colony was generated. Together, these results confirm the generation of a transgenic mouse model that over-expressed ERp57 in the central nervous system.

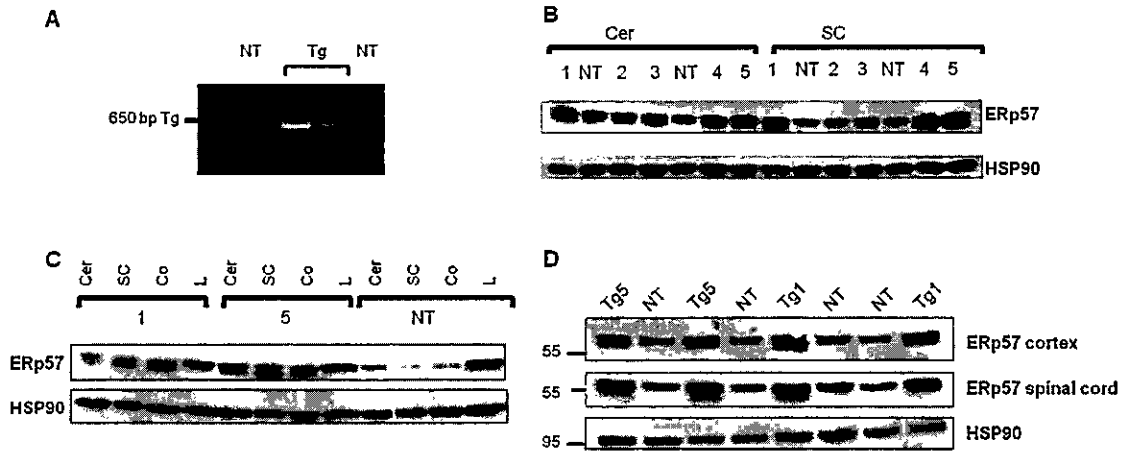

Figure 18. Characterization of ERp57 transgenic mouse lines obtained. (A) PCR analysis of genomic DNA isolated from ERp57^{Non-Tg} (NT) and transgenic (Tg) mice. Primers *erp57* 866 forward and 1535 reverse were used to obtain a 650 bp product in the case of the ERp57 transgenic or no product in case of the ERp57^{Non-Tg} mice. (B) Western blot analysis of cerebellum and spinal cord protein extracts of the F0 of 5 transgenic lines (from 1 to 5) obtained compared to ERp57^{Non-Tg} mice (NT). Lines 1 and 5 showed the highest ERp57 over-expression and were selected as the lines for amplify. (C) Western blot analyses of cerebellum, spinal cord, cortex and liver of protein samples of F0 transgenic mice line 1 and 5 compared to ERp57^{Non-Tg} mice (NT) to confirm the over-expression observed in these lines. The protein levels observed in liver were similar in transgenic and ERp57^{Non-Tg} mice. (D) Western blot analysis of cortex and spinal cord of F1 transgenic lines 1 and 5 compared to ERp57^{Non-Tg} mice (NT) to confirm that the over-expression was maintained in the generations. ERp57 protein levels were detected using an anti-ERp57 antibody. HSP90 was used as a loading control. Cer: cerebellum, SC: spinal cord, Co: cortex and L: liver, NT: Non-Tg.

Table 6. Semi-quantitative values of the Western blot analysis of cerebellum and spinal cord extracts of transgenic and ERp57^{Non-Tg} mice. The values normalized to HSP90 loading control and each ERp57^{Non-Tg} control are shown. Lines 1 and 5 displayed the highest values both in cerebellum and spinal cord and were selected to be maintained. Numbers from 1 to 5 indicates the transgenic line and NT: ERp57^{Non-Tg}.

Tissue/Line	% of NT control
Cerebellum	
1	176.5
NT	100
2	127.1
3	152.7
NT	100
4	154.8
5	182.2
Spinal cord	
1	178.8
NT	100
2	109.1
3	131.1
NT	100
4	171.6
5	201.7

7.7. Phenotypic characterization for ERp57 transgenic mice.

To investigate if the over-expression of ERp57-Flag has phenotypic effects as observed in mice with ERp57 deletion, body weight measurements, rotarod and hanging tests were performed as described here for ERp57$^{Nes-/-}$ mice. The transgenic mice appeared identical to ERp57^{Non-Tg} mice, with no obvious phenotype.

Body weight measurements were performed once a week, starting at 48 days of age of the transgenic line 5 animals and at 38 days in the transgenic line 1, until 69 or 66 days of age respectively. In Figure 19 the body weight gain by age is shown. Transgenic line 1 showed similar body weight gain curve as obtained for ERp57^{Non-Tg} mice, but transgenic line 5 showed a significant difference in body weight gain compared to ERp57^{Non-Tg} mice with an increase in the body weight.

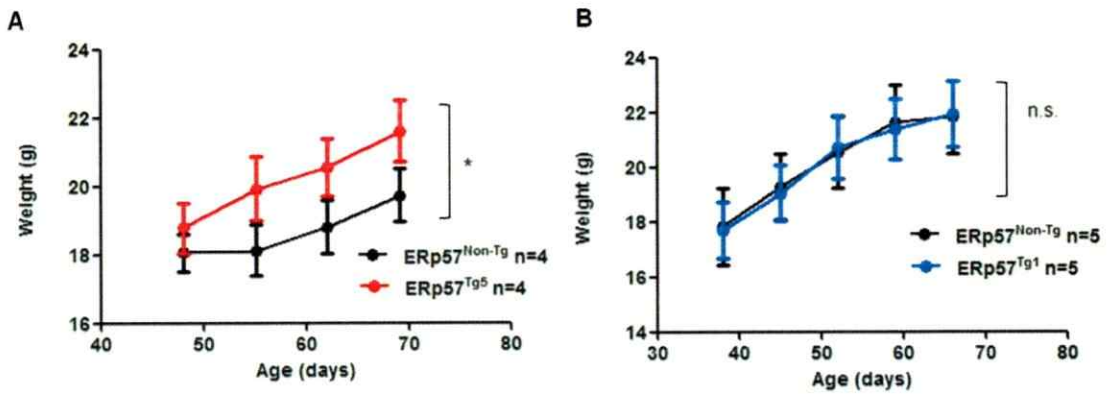

Figure 19. Body weight gain progression of ERp57^{Non-Tg} and ERp57 transgenic mice in lines 1 and 5. (A) Body weight measurements beginning at 48 days of age until 69 days once per week with n=4 ERp57^{Non-Tg} (black curve) and n=4 ERp57^{Tg5} mice (red curve). (B) Body weight measurements beginning at 38 days of age until 66 days once per week with n=5 ERp57^{Non-Tg} (black curve) and n=5 ERp57^{Tg1} mice (blue curve). Mean ± SEM of each group is shown. No difference in the body weight between ERp57^{Tg1} and ERp57^{Non-Tg} mice was found, but in the case of ERp57^{Tg5} a significant increase was found. *P* values are shown: n.s., $p>0.05$; *, $p<0.05$; Two-way ANOVA and *Bonferroni´s post hoc* test.

Rotarod tests were performed at the same age as body weight measurements for each transgenic line, and were performed every week with a constant speed of 4 rpm. In Figure 20 the result of the Rotarod test is shown, in A the times obtained for the transgenic line 5, and in B the times recorded for the transgenic line 1 mice each one compared to their ERp57^{Non-Tg} mice littermates. Because there was no difference in the performance of the Rotarod test of the Erp57-Flag transgenic mice compared to ERp57^{Non-Tg}, the Rotarod was repeated but with an increasing speed from 4 rpm to 40 rpm for 300 seconds aiming to detect possible differences between groups. Eight trials were performed in 2 consecutive days for mice of the transgenic line 1 and their ERp57^{Non-Tg} littermates (Figure 20 C). Although some points of the obtained curves differed, overall the curves were similar and no significant differences were found (Figure 20).

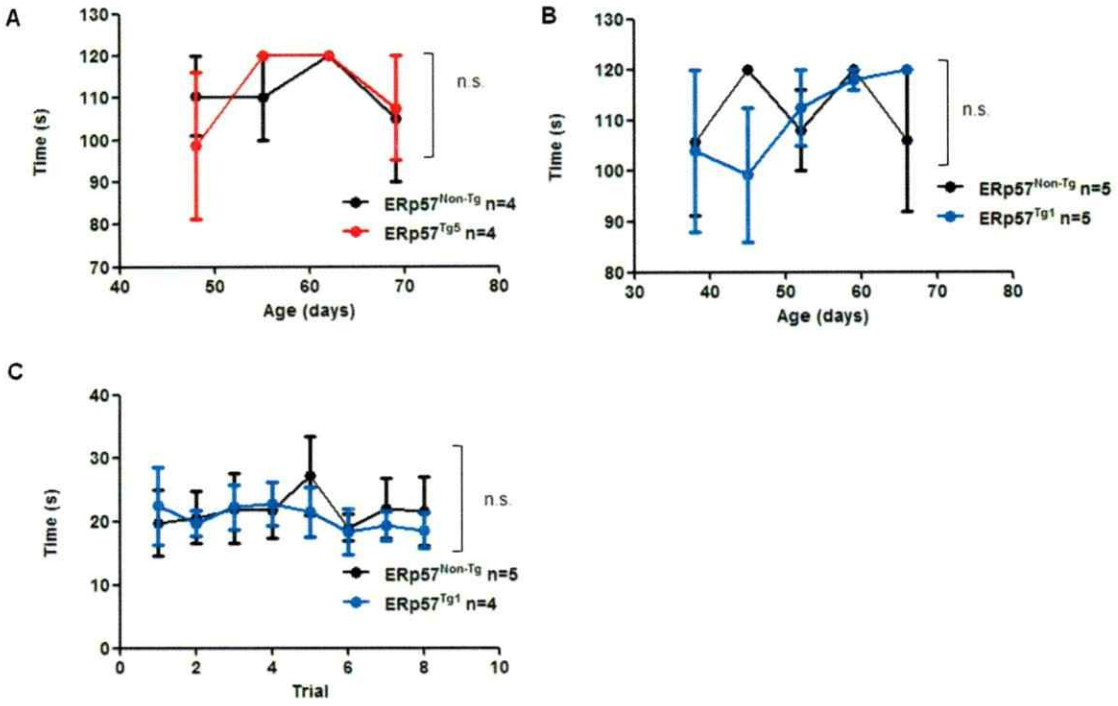

Figure 20. Rotarod performance of ERp57^{Non-Tg} and transgenic mice in lines 5 and 1. (A) Rotarod test was performed every week started at 48 days of age until 69 days with n=4 ERp57^{Non-Tg} (black curve) and n=4 ERp57^{Tg5} mice (red curve). (B) Rotarod test was performed every week started at 38 days of age until 66 days with n=5 ERp57^{Non-Tg} (black curve) and n=5 ERp57^{Tg1} mice (blue curve). (C) As there was no obvious difference, the rotarod test was done again with an acceleration speed, 8 trials in 2 consecutive days with n=5 ERp57^{Non-Tg} (black curve) and n=4 ERp57^{Tg1} mice (blue curve). With acceleration no differences appeared. Mean ± SEM of each group are shown. *P* values are shown: n.s., $p>0.05$; Two-way ANOVA and *Bonferroni´s post hoc* test.

In parallel to the measurements of the body weight and the Rotarod test, the Hanging test was also performed for transgenic mouse line 1 and 5 with their ERp57^{Non-Tg} littermates. The scores obtained for each group are shown in Figure 21. The scores obtained for the transgenic mice, in both lines 5 or 1 were similar compared to the ERp57^{Non-Tg}. All animals used for the test showed a comparable behavior and reached near the maximum score of 5. The results of the tests performed indicate that the over-expression of ERp57-Flag does not produce a motor impairment as observed in the ERp57$^{Nes-/-}$ mouse model. The phenotype of the transgenic mice was similar to that of ERp57^{Non-Tg} animals.

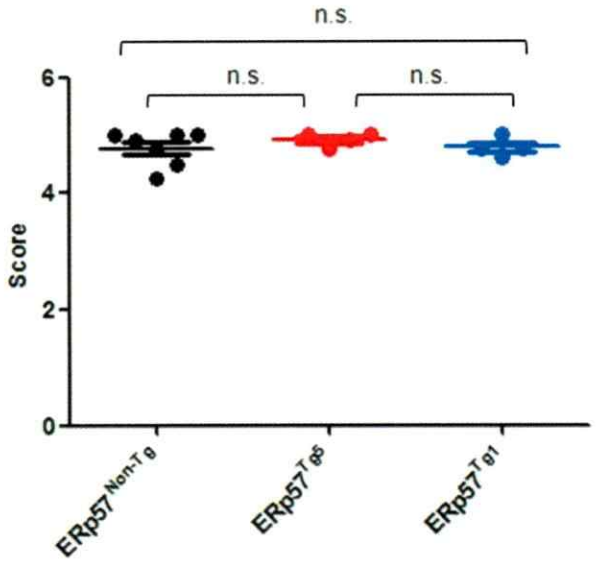

Figure 21. Hanging test scores of ERp57^{Non-Tg} and transgenic mice in lines 5 and 1. Hanging test was performed every week, the mouse was placed to hang on a horizontal bar and the reaction was recorded for 30 seconds. A score was assigned depending on the escape response of the mouse during this time with a maximum score of 5. Mean ± SEM was plotted. n=7 ERp57^{Non-Tg} (black points), n=4 ERp57^{Tg5} (red points) and n=4 ERp57^{Tg1} mice (blue points). There was no difference in the scores reached by groups; all scores recorded were near to the maximum. *P* values are shown: n.s., $p>0.05$; Student's *t*-test.

8. DISCUSSION AND CONCLUSIONS.

ERp57 is an ER foldase and chaperone, which participates in the CNX/CRT cycle and promotes folding of glycosylated proteins. As a member of the PDI family, ERp57 participates in protein disulfide bond formation and isomerization in the ER. In this thesis, we characterized two novel mouse models to manipulate ERp57: an *erp57* conditional knockout and an *erp57* transgenic mouse model in the CNS.

8.1. Motor impairment observed in the conditional *erp57* knockout mouse.

The use of a conditional *erp57* knockout mouse model provides a useful tool to study the function of ERp57 in the CNS. In previous studies it was described that the complete knockout of the *erp57* gene is embryonically lethal at stage 13.5 of development (Coe et al., 2010). Despite the absence of the protein, no effect on ER morphology, expression of other ER chaperones, ER stress levels or apoptosis were observed in ERp57 deficient MEF cells (Coe et al., 2010). A possible explanation for this phenotype could be related to the modulation of STAT3 signaling by ERp57, because STAT3 activity was increased in the absence of ERp57 and this increase in activity could contribute to embryonic lethality (Coe et al., 2010). In another study, the deletion of *erp57* specifically in B cells did not affect the development of the mouse or its viability, however ERp57 expression was found to be essential for the recruitment of MHC class I molecules to the peptide loading complex (Garbi et al., 2006), indicating a scaffold role of ERp57 in this protein complex beyond the foldase activity of ERp57. Hence the role of ERp57 in the nervous system still remained to be investigated. In this thesis, an *erp57* knockout mouse model was generated in the CNS and characterized at different levels.

To achieve *erp57* deletion in the nervous system, mice expressing the cre recombinase under the control of the nestin promoter were crossed with floxed *erp57* mice (See Material and Methods section 6.1). Nestin is an intermediate filament protein selectively expressed in neural stem cells of the developing and adult nervous system which is expressed in a wide spectrum of cell types, including neuronal and glial cells (Mignone et al., 2004). ERp57$^{Nes-/-}$ mice were generated and the loss of ERp57 was investigated in brain tissue. In all brain areas analyzed, including cortex, hippocampus and cerebellum, a dramatic reduction of ERp57 protein levels was observed in knockout mice, with an intermediate effect in heterozygous mice. These results demonstrate that *erp57* deletion was effective in the CNS. Surprisingly, the deletion also occurred in the liver, however in a lesser extent. This result demonstrates that in spite of the deletion present in the brain, it was not restricted to the CNS. Although Nestin is considered a marker of neural stem or progenitor cells in the literature, it also has been suggested that not all nestin-immunopositive cells are neural progenitor cells, and could include differentiated cells (Gilyarov, 2008). For example, nestin has been found to be expressed in other tissues, not only in the nervous system, but also in striated muscle, cardiac muscle, skin, liver, pancreas, kidney, testicles, among others (Gilyarov, 2008). Interestingly, we observed that in the liver of ERp57$^{Nes+/-}$ mice the levels of expression of *erp57* mRNA were augmented compared to the levels in the liver of ERp57^{WT} mice (data not shown), and could indicate the occurrence of a compensatory mechanism that is activated in the liver but only in the case of partial deletion of the gene in the tissue.

With respect to the rate of birth of knockout mice obtained, in all crossings the observed percentage of ERp57$^{Nes-/-}$ was lower than the expected mendelian rate of inheritance. This result could be explained by the death of some ERp57$^{Nes-/-}$ mice in utero. It may be possible that severe developmental problems were caused by the deletion of *erp57* in the nervous system already in utero. Overall, a reduction in body weight and

defects in motor coordination of knockout and heterozygous mice were determinated by visual observation and locomotor coordination tests, including the Rotarod and Hanging test, which demonstrated that reduced ERp57 levels led to motor impairment, which was observed as early as 20 days of age.

The body weight reduction was more severe when knockout and heterozygous mice were analyzed at a younger age (since 20 days of age until 120 days), compared to wildtype mice. At a later age, differences were maintained but became less pronounced. This severe decrease in the growth rate of the $ERp57^{Nes-/-}$ mice and the mild decrease of size of $ERp57^{Nes+/-}$ mice could be caused by a developmental defect, because it was already apparent at birth. Given that the first days after birth are critical days to receive enough nutrition, it could be possible that the motor and cognitive problems could have been at least partially prevented by more feeding. Also, it has been described that ER stress and the UPR pathway in hypothalamus have an important role in leptin signaling, a hormone that regulates appetite and growth metabolism (Ozcan et al., 2009), which may be affected by ERp57 deficiency. Furthermore, chemical chaperones act as leptin-sensitizing agents and could be useful for obesity treatments (Ozcan et al., 2009). We speculate that it may be possible to explain the body weight reduction of *erp57* knockout mice with an ER stress modulation in hypothalamic neurons that may change leptin regulation.

Together, the Rotarod test and Hanging test indicate severe motor coordination problems in $ERp57^{Nes-/-}$ mice, since in both tests $ERp57^{Nes-/-}$ animals performed close to the minimum measurable (a few seconds in the Rotarod test and scores near to 1 in the Hanging test). In spite of this, visual observation of mice indicated no signs of paralysis or strong motor defects. This motor impairment had no age-dependency since it already started when the mouse was a new born pup and no progression over time.

In light of the results of the motor tests performed, another test was included in the analysis, the Footprinting assay. This test is extensively used to assess the consequences of spinal cord injury or nerve damage. Visually, the footprints of $ERp57^{Nes-/-}$ mice and $ERp57^{Nes+/-}$ mice were not drastically different when compared to wildtype mice. Several parameters obtained with the footprint assay were quantified including the hindlimb angle of rotation, the interlimb coordination and the distance between limbs, based on Karimi-Abdolrezaee et al., 2006. No significant differences between $ERp57^{Nes-/-}$ mice and $ERp57^{WT}$ mice were found in any of the measurements performed. These results indicate that mice deficient in ERp57 do not display strong alterations in fine movements, as it would be expected in the case of nerve damage for example. The footprinting assay in this case was not appropriate to demonstrate non-servere motor problems.

Consistent with the findings obtained in conditional *erp57* knockout mice, all the $ERp57^{Nes-/-}$ and some of the $ERp57^{Nes+/-}$ mice analyzed showed PSW with a score of +1 in the EMG analysis, unlike $ERp57^{WT}$ mice that did not show PSW, and therefore received, a score of 0. PSW as an indicator of the loss of muscle fiber innervations, which is commonly observed in ALS patients (Inghilleri and Iacovelli, 2011) or in transgenic mice that developed features of ALS (Wegorzewska et al., 2009). These results demonstrate that ERp57 deficient mice had muscle denervation. Denervation occurs when the connection between nerve and muscle is interrupted and the muscle no longer receives stimuli from the nervous system. The cause of this denervation in our model needs to be further investigated, since it may indicate dysfunction or disease states at the central nervous system, peripheral nervous system or at the muscle. For example, alterations at the synaptic terminal of the nerve, modified levels of expression of some receptors or of proteins present in the muscle could lead to a loss of synapsis and/or communication between nerve and muscle. Based on studies on CNX deficient mice (Denzel et al., 2002; Kraus et al., 2010), it may be also possible that myelin folding and/or synthesis may be

altered in ERp57 deficient animals. It is important to mention that in the ERp57 deficient mice this denervation was not found in all measurements, unlike in transgenic $SOD1^{G86R}$ late disease stage mice.

It is interesting to note that *bip* knockout mice, SIL1 mutant and CNX deficient mouse models showed motor impairment (Denzel et al., 2002; Kraus et al., 2010; Wang et al., 2010; Zhao et al., 2005) very similar to the phenotype observed of *erp57* conditional knockout mouse model. *Bip* knockout mice also presented with growth retardation, ataxia and a severe defect in motor coordination assessed by body weight and food consumption as well as Rotarod and Footprinting tests (Wang et al., 2010). SIL1 mutant mice also developed ataxia (Zhao et al., 2005). Furthermore, CNX deficient mice were smaller than wildtype (Denzel et al., 2002; Kraus et al., 2010) and showed severe body shaking and behavioral abnormalities (Denzel et al., 2002). Thus, the deficiency of ER chaperones and foldases, like ERp57, BIP or CNX, leads to similar phenotypes in mice, although probably due to different mechanisms. The *bip* knockout was specific for PC and the mice showed cerebellar atrophy with an accelerated degeneration in the PC associated with increased apoptosis levels and upregulated ER stress markers (Wang et al., 2010). SIL1 mutant mice showed PC loss and abnormal accumulation of ubiquitinated proteins in PC associated with ER stress. This mouse model highlights the presence of ubiquitinated protein aggregates (Zhao et al., 2005), which was not seen in the other mouse models discussed. This ubiquitination could have an important role in the phenotype observed, directly relating ER stress with neurodegeneration due to accumulation of toxic protein aggregates. CNX deficient mice on the other hand, displayed first a dramatic loss of large myelinated nerve fibers and second a dysmyelination leading to myelinopathy (Denzel et al., 2002; Kraus et al., 2010). Thus, each ER chaperone deficient mouse model displayed a specific cell population altered, like PC of cerebellum or nerve fibers. These results suggest that each ER chaperone may have more fundamental functions in particular brain

areas. This may be explained because each chaperone has its own set of substrates altering distinct neuronal populations. In the case of *erp57* knockout mice, the mechanism of the motor impairment remains unknown.

8.2. Possible mechanism of motor impairment in the *erp57* knockout mouse.

In order to identify a possible mechanism that may explain the motor impairment observed in the ERp57 deficient mice, the cellular environment and the protein homeostasis network was analyzed. As mentioned previously, PC specific *bip* knockout mice displayed a similar phenotype as described here for ERp57 deficient mice. In this case cerebellar atrophy occurred, demonstrating that BIP is essential for survival of PC and the integrity of the cerebellum (Wang et al., 2010). Because the cerebellum is an area of the brain that plays an important role in motor control and movement-related functions, contributing to coordination and precision; an immunohistochemistry with Calbindin, a marker of PC was performed. The number of cerebellar lobules, PC and layers was quantified in $ERp57^{Nes-/-}$ and $ERp57^{WT}$ mice. No difference was observed between the genotypes. We speculate that the motor impairment observed was not due to neuronal loss in the cerebellum. However, we cannot discard possible effects on neuronal functionality that could trigger motor defects. The motor phenotype could also be associated with alterations in another brain area like the motor cortex.

The number of neurons of the ventral horn with morphology of motoneurons was quantified and a slight but significant decrease of motoneuron number was found in the $ERp57^{Nes-/-}$ mice compared to $ERp57^{WT}$. In addition, the relative size of neurons was quantified, however, no difference was found. Overall the slight reduction in motoneuron number and the mild muscle denervation observed in $ERp57^{Nes-/-}$ mice is consistent with the motor impairment observed. In this context the lack of ERp57 in spinal cord could lead to alterations in ER homeostasis and protein folding affecting the ER function, triggering

apoptosis or degeneration of neurons. Together with the muscle denervation analyzed by EMG, these results demonstrate a fundamental role of ERp57 in the control of motor function of the nervous system. However, additional experiments should be performed to understand the molecular mechanism of how ERp57 affects motor functions.

To analyze if the lack of ERp57 resulted in an alteration in protein homeostasis, we monitored the levels of several ER chaperones, foldases, and PDI family members in cortex, hippocampus, cerebellum and liver. We measured the levels of: ERO1, an ER oxidoreductin protein that has been proposed as a main participant in the recycling of PDI and possibly ERp57 to their active state (Appenzeller-Herzog et al., 2010; Tavender and Bulleid, 2010); PDI, having the highest homology to ERp57 (Maattanen et al., 2006); ERp72, which possible can compensate for the loss of ERp57 (Solda et al., 2006); CNX, another ER chaperone interacting with ERp57 to promote folding of glycoproteins (Ellgaard and Frickel, 2003); and BIP, an ER chaperone that is regulated by the UPR (Hetz, 2012).

In conclusion, most of the ER foldases and chaperones analyzed were reduced in cortex and cerebellum of $ERp57^{Nes-/-}$ mice but increased in hippocampus with the exception of ERp72. Since each tissue may display differential regulation of protein expression to fulfill specific folding demands, it is expected to observe differential responses to the lack of one particular foldase in each tissue, in this case ERp57.

Thus, the lack of ERp57 in the brain resulted in a shift in the protein homeostasis network, which might be due to deficient glycoprotein folding in the ER. Contrary to our expectations according to the literature (Solda et al., 2006), no compensation by PDI or ERp72 up-regulation was found. Also, no basal levels of ER stress or increased UPR activation were observed at least with the experiments performed in the course of this thesis based on BIP protein levels. Further experiments are needed to determine if under acute ER stress, ERp57 deficient mice display an altered UPR. Since BIP and CNX were

decreased in cortex and cerebellum, tissues that have important role in motor functions, it is possible that this decrease, similar to *bip* and *cnx* knockout mice contributes to the phenotype observed due to altered ER function. Interestingly, this decrease was not observed in hippocampus, a tissue that is related with memory and learning function.

We speculate that the abnormal protein homeostasis caused by the lack of ERp57 could generate toxic effects in neurons originating in the failure to efficiently and correctly fold key proteins trafficking through the ER, such as receptors or synaptic terminal proteins or also myelin synthesis. As a consequence connections between neurons and muscle cells are terminated or the cell death pathways are activated. Future studies on primary neurons derived from ERp57 deficient mice, should give insights about the molecular mechanisms leading to the motor phenotype observed in these animals.

8.3. ERp57 transgenic mouse model.

Considering the results obtained for the *erp57* knockout mouse model, another mouse model was generated that over-expresses ERp57-Flag in the CNS, an ERp57 transgenic mouse. The future use of this model is to test possible therapeutic effects of over-expressing this protein in diverse disease settings. Targeted expression of ERp57 in the nervous system was achieved by using the Prion promoter. Prion protein has high levels of expression in nervous tissues (Ford et al., 2002; Linden et al., 2008) and has been widely used to direct the expression to the brain in transgenic animals (Waldron-Roby et al., 2012).

The possible phenotype of the ERp57-Flag transgenic mice was analyzed in the same way as performed for the *erp57* conditional knockout mice. No visual difference between ERp57 transgenic and wildtype mice was observed. Body weight measurements, Rotarod and Hanging test performances of both transgenic lines did not show any difference to the wildtype animals, indicating that the over-expression of ERp57 resulted in a normal

phenotype, at least under the tested conditions. Although a slight significative difference was found in transgenic line 5 body weight. It is possible that the over-expression of ERp57 may promote an improvement in the performance in certain tests; however the assays performed here are mainly designed to assess a worsening of the phenotype rather than an improvement.

ERp57 transgenic mice may have a different response to ER stress conditions associated with neurodegeneration. Therefore experiments to induce ER stress *in vivo* (Adachi et al., 2011; Lee et al., 2012) or in primary neuron culture (Goslin, 1991; Hetz et al., 2008) could give great insights into its function in pathology. Collectively, we would expect a protective effect of the over-expression of ERp57 under ER stress. The experiments with the primary culture of cortical neurons from transgenic and wildtype mice are in progress in our laboratory. Preliminary results indeed indicate that ERp57 over-expression confers resistance to ER stress (data not shown) however more experiments are necessary to ascertain this observation.

8.4. ERp57 in neurological pathologies.

In this *in vivo* study the relation between protein folding in the ER and neuronal dysfunction was evidenced. ER stress is associated to the abnormal protein aggregation process and cell degeneration observed in many neurodegenerative diseases, including ALS, AD, HD, PD and PrDs (Matus et al., 2011). ERp57 has been described to be induced in the brain of important neurodegenerative diseases, including ALS, AD, PrDs and HD in cellular, animal models and human patient samples (Atkin et al., 2006; Hetz et al., 2009; Massignan et al., 2007; Erickson et al., 2005; Hoffstrom et al., 2010; Hetz et al., 2003; Hetz et al., 2005). For example, in ALS patients and SOD1 mutant transgenic rats ERp57 was found to be up-regulated in the spinal cord (Atkin et al., 2006; Hetz et al., 2009; Massignan et al., 2007). In AD, it was also described that ERp57 interacts with β-amyloid

in cerebrospinal fluid (CSF) preventing its aggregation (Erickson et al., 2005). On the other hand, in CJD patients (Hetz et al., 2003; Yoo et al., 2002), ERp57 was found to be over-expressed, which was also recapitulated in murine scrapie strain 139A (Hetz et al., 2003). The knockdown of ERp57 increases Prion toxicity and over-expression leads to the opposite result (Hetz et al., 2005). These results suggest a protective role of ERp57 in neurodegenerative pathologies. In the other hand, the inhibition of ERp57 and PDI had a protective effect in neurodegeneration associated with amyloid precursors and polyglutamines *in vitro* (Hoffstrom et al., 2010), suggesting a pro-apoptotic role of ERp57 in AD and HD. However, most of the studies linking ERp57 with neurodegeneration *in vivo* are correlative and functional data, in disease conditions has been only provided *in vitro*. The generation of the two mouse models to study ERp57 function *in vivo* open the possibility for investigating for the first time the functional contribution of ERp57 to important neurodegenerative diseases.

To corroborate the *in vitro* data and clarify the possible role of ERp57 in neurodegenerative diseases, additional *in vivo* studies are necessary. ERp57 was found to be an important marker for ALS progression (Nardo et al., 2011), and possibly its modulation would be a key element for studies to develop treatments for the neurodegenerative diseases in which ERp57 has been associated. Mouse models with manipulated expression of ERp57 *in vivo* then constitute useful tools to analyze in the future its contribution to neurodegeneration also in a disease context. In summary, this thesis constitutes the first study investigating the role of a PDI family member in the nervous system, identifying an important function of ERp57 in the control of motor activity.

9. PROJECTIONS.

This study constitutes the first characterization of an *erp57* knockout mouse model and describes causes of the motor impairment observed. Further experiments are necessary to complete this characterization, including for example the analysis of the complete brain by histology and the assessment of the level of neurodegeneration and apoptosis in the *erp57* conditional knockout mice.

In addition, the exposure of either mice or cultured neurons to ER stress could potentially answer many questions regarding the mechanism of the motor impairment observed. Also, it will be very interesting to investigate if ERp57 knockout or transgenic mice have a different response to important neurodegenerative diseases, a question which could be studied by infecting these mice with the scrapie form of the prion protein or by crossing them with mice displaying the ALS phenotype, like mice expressing the SOD1 mutant. Since the lack of ERp57 leads to motor impairment similar to the ALS phenotype, experiments should be performed with the ERp57 transgenic mice.

In the case of *erp57* conditional knockout mice, cognitive tests can also be performed to analyze the contribution of this protein in memory and other hippocampal functions, especially since recent evidence relates ERp57 with AD.

In the case of the transgenic mice, many experiments can be proposed; first the possible resistance to ER stress or an altered response to ER stress has to be investigated. Especially preliminary experiments using ER stress in primary cortical neurons derived from ERp57 transgenic mice indicate that this will be an interesting line of investigation. If neuronal protection is confirmed, crossing ERp57 transgenic mice with transgenic mice expressing mutant SOD1, a model for ALS, promises to protect the offspring from disease development and/or progression.

10. REFERENCES.

Adachi, T., Yasuda, H., Nakamura, S., Kamiya, T., Hara, H., Hara, H., and Ikeda, T. (2011). Endoplasmic reticulum stress induces retinal endothelial permeability of extracellular-superoxide dismutase. Free Radic Res *45*, 1083-1092.

Appenzeller-Herzog, C., and Ellgaard, L. (2008). The human PDI family: versatility packed into a single fold. Biochim Biophys Acta *1783*, 535-548.

Appenzeller-Herzog, C., Riemer, J., Zito, E., Chin, K. T., Ron, D., Spiess, M., and Ellgaard, L. (2010). Disulphide production by Ero1alpha-PDI relay is rapid and effectively regulated. Embo J *29*, 3318-3329.

Atkin, J. D., Farg, M. A., Turner, B. J., Tomas, D., Lysaght, J. A., Nunan, J., Rembach, A., Nagley, P., Beart, P. M., Cheema, S. S., and Horne, M. K. (2006). Induction of the unfolded protein response in familial amyotrophic lateral sclerosis and association of protein-disulfide isomerase with superoxide dismutase 1. J Biol Chem *281*, 30152-30165.

Atkin, J. D., Farg, M. A., Walker, A. K., McLean, C., Tomas, D., and Horne, M. K. (2008). Endoplasmic reticulum stress and induction of the unfolded protein response in human sporadic amyotrophic lateral sclerosis. Neurobiol Dis *30*, 400-407.

Benham, A. M. (2012). The protein disulfide isomerase family: key players in health and disease. Antioxid Redox Signal *16*, 781-789.

Borchelt, D. R., Davis, J., Fischer, M., Lee, M. K., Slunt, H. H., Ratovitsky, T., Regard, J., Copeland, N. G., Jenkins, N. A., Sisodia, S. S., and Price, D. L. (1996). A vector for expressing foreign genes in the brains and hearts of transgenic mice. Genet Anal *13*, 159-163.

Coe, H., Jung, J., Groenendyk, J., Prins, D., and Michalak, M. (2010). ERp57 modulates STAT3 signaling from the lumen of the endoplasmic reticulum. J Biol Chem *285*, 6725-6738.

Coe, H., and Michalak, M. (2010). ERp57, a multifunctional endoplasmic reticulum resident oxidoreductase. Int J Biochem Cell Biol *42*, 796-799.

Coppari, S., Altieri, F., Ferraro, A., Chichiarelli, S., Eufemi, M., and Turano, C. (2002). Nuclear localization and DNA interaction of protein disulfide isomerase ERp57 in mammalian cells. J Cell Biochem *85*, 325-333.

Chen, X., Shen, J., and Prywes, R. (2002). The luminal domain of ATF6 senses endoplasmic reticulum (ER) stress and causes translocation of ATF6 from the ER to the Golgi. J Biol Chem *277*, 13045-13052.

Chipuk, J. E., Bouchier-Hayes, L., and Green, D. R. (2006). Mitochondrial outer membrane permeabilization during apoptosis: the innocent bystander scenario. Cell Death Differ *13*, 1396-1402.

Denisov, A. Y., Maattanen, P., Dabrowski, C., Kozlov, G., Thomas, D. Y., and Gehring, K. (2009). Solution structure of the bb' domains of human protein disulfide isomerase. Febs J *276*, 1440-1449.

Denzel, A., Molinari, M., Trigueros, C., Martin, J. E., Velmurgan, S., Brown, S., Stamp, G., and Owen, M. J. (2002). Early postnatal death and motor disorders in mice congenitally deficient in calnexin expression. Mol Cell Biol *22*, 7398-7404.

Dong, G., Wearsch, P. A., Peaper, D. R., Cresswell, P., and Reinisch, K. M. (2009). Insights into MHC class I peptide loading from the structure of the tapasin-ERp57 thiol oxidoreductase heterodimer. Immunity *30*, 21-32.

Dorner, A. J., Wasley, L. C., Raney, P., Haugejorden, S., Green, M., and Kaufman, R. J. (1990). The stress response in Chinese hamster ovary cells. Regulation of ERp72 and protein disulfide isomerase expression and secretion. J Biol Chem *265*, 22029-22034.

Ellgaard, L., and Frickel, E. M. (2003). Calnexin, calreticulin, and ERp57: teammates in glycoprotein folding. Cell Biochem Biophys *39*, 223-247.

Ellgaard, L., and Ruddock, L. W. (2005). The human protein disulphide isomerase family: substrate interactions and functional properties. EMBO Rep *6*, 28-32.

Erickson, R. R., Dunning, L. M., Olson, D. A., Cohen, S. J., Davis, A. T., Wood, W. G., Kratzke, R. A., and Holtzman, J. L. (2005). In cerebrospinal fluid ER chaperones ERp57 and calreticulin bind beta-amyloid. Biochem Biophys Res Commun *332*, 50-57.

Feige, M. J., and Hendershot, L. M. (2011). Disulfide bonds in ER protein folding and homeostasis. Curr Opin Cell Biol *23*, 167-175.

Ferrari, D. M., and Soling, H. D. (1999). The protein disulphide-isomerase family: unravelling a string of folds. Biochem J *339 (Pt 1)*, 1-10.

Ford, M. J., Burton, L. J., Morris, R. J., and Hall, S. M. (2002). Selective expression of prion protein in peripheral tissues of the adult mouse. Neuroscience *113*, 177-192.

Garbi, N., Tanaka, S., Momburg, F., and Hammerling, G. J. (2006). Impaired assembly of the major histocompatibility complex class I peptide-loading complex in mice deficient in the oxidoreductase ERp57. Nat Immunol *7*, 93-102.

Germain, M., and Shore, G. C. (2003). Cellular distribution of Bcl-2 family proteins. Sci STKE *2003*, pe10.

Gilyarov, A. V. (2008). Nestin in central nervous system cells. Neurosci Behav Physiol *38*, 165-169.

Goslin, K., Banker, G. (1991). Rat hippocampal neurons in low-density cultures. Culturing nerve cells, Banker G, Goslin K, eds, Cambridge, MA, MIT, 251-281.

Grubb, S., Guo, L., Fisher, E. A., and Brodsky, J. L. (2012). Protein disulfide isomerases contribute differentially to the endoplasmic reticulum-associated degradation of apolipoprotein B and other substrates. Mol Biol Cell *23*, 520-532.

Guo, G. G., Patel, K., Kumar, V., Shah, M., Fried, V. A., Etlinger, J. D., and Sehgal, P. B. (2002). Association of the chaperone glucose-regulated protein 58 (GRP58/ER-60/ERp57) with Stat3 in cytosol and plasma membrane complexes. J Interferon Cytokine Res *22*, 555-563.

Harding, H. P., Zhang, Y., Zeng, H., Novoa, I., Lu, P. D., Calfon, M., Sadri, N., Yun, C., Popko, B., Paules, R., *et al.* (2003). An integrated stress response regulates amino acid metabolism and resistance to oxidative stress. Mol Cell *11*, 619-633.

Hatahet, F., and Ruddock, L. W. (2009). Protein disulfide isomerase: a critical evaluation of its function in disulfide bond formation. Antioxid Redox Signal *11*, 2807-2850.

Hetz, C. (2012). The unfolded protein response: controlling cell fate decisions under ER stress and beyond. Nat Rev Mol Cell Biol *13*, 89-102.

Hetz, C., Lee, A. H., Gonzalez-Romero, D., Thielen, P., Castilla, J., Soto, C., and Glimcher, L. H. (2008). Unfolded protein response transcription factor XBP-1 does not influence prion replication or pathogenesis. Proc Natl Acad Sci U S A *105*, 757-762.

Hetz, C., Martinon, F., Rodriguez, D., and Glimcher, L. H. (2011). The Unfolded Protein Response: Integrating Stress Signals Through the Stress Sensor IRE1{alpha}. Physiol Rev *91*, 1219-1243.

Hetz, C., Russelakis-Carneiro, M., Maundrell, K., Castilla, J., and Soto, C. (2003). Caspase-12 and endoplasmic reticulum stress mediate neurotoxicity of pathological prion protein. EMBO J *22*, 5435-5445.

Hetz, C., Russelakis-Carneiro, M., Walchli, S., Carboni, S., Vial-Knecht, E., Maundrell, K., Castilla, J., and Soto, C. (2005). The disulfide isomerase Grp58 is a protective factor against prion neurotoxicity. J Neurosci *25*, 2793-2802.

Hetz, C., Thielen, P., Matus, S., Nassif, M., Court, F., Kiffin, R., Martinez, G., Cuervo, A. M., Brown, R. H., and Glimcher, L. H. (2009). XBP-1 deficiency in the nervous system protects against amyotrophic lateral sclerosis by increasing autophagy. Genes Dev *23*, 2294-2306.

Hirano, N., Shibasaki, F., Sakai, R., Tanaka, T., Nishida, J., Yazaki, Y., Takenawa, T., and Hirai, H. (1995). Molecular cloning of the human glucose-regulated protein ERp57/GRP58, a thiol-dependent reductase. Identification of its secretory form and inducible expression by the oncogenic transformation. Eur J Biochem *234*, 336-342.

Hoffstrom, B. G., Kaplan, A., Letso, R., Schmid, R. S., Turmel, G. J., Lo, D. C., and Stockwell, B. R. (2010). Inhibitors of protein disulfide isomerase suppress apoptosis induced by misfolded proteins. Nat Chem Biol *6*, 900-906.

Honjo, Y., Ito, H., Horibe, T., Takahashi, R., and Kawakami, K. (2010). Protein disulfide isomerase-immunopositive inclusions in patients with Alzheimer disease. Brain Res *1349*, 90-96.

Hosoda, A., Tokuda, M., Akai, R., Kohno, K., and Iwawaki, T. (2010). Positive contribution of ERdj5/JPDI to endoplasmic reticulum protein quality control in the salivary gland. Biochem J *425*, 117-125.

Inghilleri, M., and Iacovelli, E. (2011). Clinical neurophysiology in ALS. Arch Ital Biol *149*, 57-63.

Jellinger, K. A. (2010). Basic mechanisms of neurodegeneration: a critical update. J Cell Mol Med *14*, 457-487.

Jessop, C. E., Chakravarthi, S., Garbi, N., Hammerling, G. J., Lovell, S., and Bulleid, N. J. (2007). ERp57 is essential for efficient folding of glycoproteins sharing common structural domains. Embo J *26*, 28-40.

Karimi-Abdolrezaee, S., Eftekharpour, E., Wang, J., Morshead, C. M., and Fehlings, M. G. (2006). Delayed transplantation of adult neural precursor cells promotes remyelination and functional neurological recovery after spinal cord injury. J Neurosci *26*, 3377-3389.

Khanal, R. C., and Nemere, I. (2007). The ERp57/GRp58/1,25D3-MARRS receptor: multiple functional roles in diverse cell systems. Curr Med Chem *14*, 1087-1093.

Kim, S., Wang, M., Lee, A. S., and Thompson, R. F. (2011). Impaired eyeblink conditioning in 78 kDa-glucose regulated protein (GRP78)/immunoglobulin binding protein (BiP) conditional knockout mice. Behav Neurosci *125*, 404-411.

Koivunen, P., Horelli-Kuitunen, N., Helaakoski, T., Karvonen, P., Jaakkola, M., Palotie, A., and Kivirikko, K. I. (1997). Structures of the human gene for the protein disulfide isomerase-related polypeptide ERp60 and a processed gene and assignment of these genes to 15q15 and 1q21. Genomics *42*, 397-404.

Kozlov, G., Maattanen, P., Schrag, J. D., Pollock, S., Cygler, M., Nagar, B., Thomas, D. Y., and Gehring, K. (2006). Crystal structure of the bb' domains of the protein disulfide isomerase ERp57. Structure *14*, 1331-1339.

Kozlov, G., Maattanen, P., Thomas, D. Y., and Gehring, K. (2010). A structural overview of the PDI family of proteins. Febs J *277*, 3924-3936.

Kraus, A., Groenendyk, J., Bedard, K., Baldwin, T. A., Krause, K. H., Dubois-Dauphin, M., Dyck, J., Rosenbaum, E. E., Korngut, L., Colley, N. J., *et al.* (2010). Calnexin deficiency leads to dysmyelination. J Biol Chem *285*, 18928-18938.

Lee, J. S., Zheng, Z., Mendez, R., Ha, S. W., Xie, Y., and Zhang, K. (2012). Pharmacologic ER stress induces non-alcoholic steatohepatitis in an animal model. Toxicol Lett.

Linden, R., Martins, V. R., Prado, M. A., Cammarota, M., Izquierdo, I., and Brentani, R. R. (2008). Physiology of the prion protein. Physiol Rev *88*, 673-728.

Luo, S., Mao, C., Lee, B., and Lee, A. S. (2006). GRP78/BiP is required for cell proliferation and protecting the inner cell mass from apoptosis during early mouse embryonic development. Mol Cell Biol *26*, 5688-5697.

Maattanen, P., Gehring, K., Bergeron, J. J., and Thomas, D. Y. (2010). Protein quality control in the ER: the recognition of misfolded proteins. Semin Cell Dev Biol *21*, 500-511.

Maattanen, P., Kozlov, G., Gehring, K., and Thomas, D. Y. (2006). ERp57 and PDI: multifunctional protein disulfide isomerases with similar domain architectures but differing substrate-partner associations. Biochem Cell Biol *84*, 881-889.

Massignan, T., Casoni, F., Basso, M., Stefanazzi, P., Biasini, E., Tortarolo, M., Salmona, M., Gianazza, E., Bendotti, C., and Bonetto, V. (2007). Proteomic analysis of spinal cord of presymptomatic amyotrophic lateral sclerosis G93A SOD1 mouse. Biochem Biophys Res Commun *353*, 719-725.

Matus, S., Glimcher, L. H., and Hetz, C. (2011). Protein folding stress in neurodegenerative diseases: a glimpse into the ER. Curr Opin Cell Biol *23*, 239-252.

Mesaeli, N., Nakamura, K., Zvaritch, E., Dickie, P., Dziak, E., Krause, K. H., Opas, M., MacLennan, D. H., and Michalak, M. (1999). Calreticulin is essential for cardiac development. J Cell Biol *144*, 857-868.

Mignone, J. L., Kukekov, V., Chiang, A. S., Steindler, D., and Enikolopov, G. (2004). Neural stem and progenitor cells in nestin-GFP transgenic mice. J Comp Neurol *469*, 311-324.

Mukherjee, A., and Soto, C. (2011). Role of calcineurin in neurodegeneration produced by misfolded proteins and endoplasmic reticulum stress. Curr Opin Cell Biol *23*, 223-230.

Nardo, G., Pozzi, S., Pignataro, M., Lauranzano, E., Spano, G., Garbelli, S., Mantovani, S., Marinou, K., Papetti, L., Monteforte, M., *et al.* (2011). Amyotrophic lateral sclerosis multiprotein biomarkers in peripheral blood mononuclear cells. PLoS One *6*, e25545.

Nemere, I., Garbi, N., Hammerling, G. J., and Khanal, R. C. (2010). Intestinal cell calcium uptake and the targeted knockout of the 1,25D3-MARRS (membrane-associated, rapid response steroid-binding) receptor/PDIA3/Erp57. J Biol Chem *285*, 31859-31866.

Ni, M., and Lee, A. S. (2007). ER chaperones in mammalian development and human diseases. FEBS Lett *581*, 3641-3651.

Ozcan, L., Ergin, A. S., Lu, A., Chung, J., Sarkar, S., Nie, D., Myers, M. G., Jr., and Ozcan, U. (2009). Endoplasmic reticulum stress plays a central role in development of leptin resistance. Cell Metab *9*, 35-51.

Park, S. W., Zhen, G., Verhaeghe, C., Nakagami, Y., Nguyenvu, L. T., Barczak, A. J., Killeen, N., and Erle, D. J. (2009). The protein disulfide isomerase AGR2 is essential for production of intestinal mucus. Proc Natl Acad Sci U S A *106*, 6950-6955.

Pirneskoski, A., Klappa, P., Lobell, M., Williamson, R. A., Byrne, L., Alanen, H. I., Salo, K. E., Kivirikko, K. I., Freedman, R. B., and Ruddock, L. W. (2004). Molecular characterization of the principal substrate binding site of the ubiquitous folding catalyst protein disulfide isomerase. J Biol Chem *279*, 10374-10381.

Rodriguez, D., Rojas-Rivera, D., and Hetz, C. (2011). Integrating stress signals at the endoplasmic reticulum: The BCL-2 protein family rheostat. Biochim Biophys Acta *1813*, 564-574.

Ron, D., and Walter, P. (2007). Signal integration in the endoplasmic reticulum unfolded protein response. Nat Rev Mol Cell Biol *8*, 519-529.

Rubinsztein, D. C., Marino, G., and Kroemer, G. (2011). Autophagy and aging. Cell *146*, 682-695.

Rutkevich, L. A., Cohen-Doyle, M. F., Brockmeier, U., and Williams, D. B. (2010). Functional relationship between protein disulfide isomerase family members during the oxidative folding of human secretory proteins. Mol Biol Cell *21*, 3093-3105.

Rutkevich, L. A., and Williams, D. B. (2011). Participation of lectin chaperones and thiol oxidoreductases in protein folding within the endoplasmic reticulum. Curr Opin Cell Biol *23*, 157-166.

Schroder, M., and Kaufman, R. J. (2005). The mammalian unfolded protein response. Annu Rev Biochem *74*, 739-789.

Solda, T., Garbi, N., Hammerling, G. J., and Molinari, M. (2006). Consequences of ERp57 deletion on oxidative folding of obligate and facultative clients of the calnexin cycle. J Biol Chem *281*, 6219-6226.

Soto, C. (2003). Unfolding the role of protein misfolding in neurodegenerative diseases. Nat Rev Neurosci *4*, 49-60.

Tait, S. W., and Green, D. R. (2010). Mitochondria and cell death: outer membrane permeabilization and beyond. Nat Rev Mol Cell Biol *11*, 621-632.

Tavender, T. J., and Bulleid, N. J. (2010). Molecular mechanisms regulating oxidative activity of the Ero1 family in the endoplasmic reticulum. Antioxid Redox Signal *13*, 1177-1187.

Tian, G., Kober, F. X., Lewandrowski, U., Sickmann, A., Lennarz, W. J., and Schindelin, H. (2008). The catalytic activity of protein-disulfide isomerase requires a conformationally flexible molecule. J Biol Chem *283*, 33630-33640.

Tian, G., Xiang, S., Noiva, R., Lennarz, W. J., and Schindelin, H. (2006). The crystal structure of yeast protein disulfide isomerase suggests cooperativity between its active sites. Cell *124*, 61-73.

Tu, B. P., and Weissman, J. S. (2002). The FAD- and O(2)-dependent reaction cycle of Ero1-mediated oxidative protein folding in the endoplasmic reticulum. Mol Cell *10*, 983-994.

Turano, C., Coppari, S., Altieri, F., and Ferraro, A. (2002). Proteins of the PDI family: unpredicted non-ER locations and functions. J Cell Physiol *193*, 154-163.

Uehara, T., Nakamura, T., Yao, D., Shi, Z. Q., Gu, Z., Ma, Y., Masliah, E., Nomura, Y., and Lipton, S. A. (2006). S-nitrosylated protein-disulphide isomerase links protein misfolding to neurodegeneration. Nature *441*, 513-517.

Waldron-Roby, E., Ratovitski, T., Wang, X., Jiang, M., Watkin, E., Arbez, N., Graham, R. K., Hayden, M. R., Hou, Z., Mori, S., *et al.* (2012). Transgenic mouse model expressing the caspase 6 fragment of mutant huntingtin. J Neurosci *32*, 183-193.

Walker, A. K., Farg, M. A., Bye, C. R., McLean, C. A., Horne, M. K., and Atkin, J. D. (2010). Protein disulphide isomerase protects against protein aggregation and is S-nitrosylated in amyotrophic lateral sclerosis. Brain *133*, 105-116.

Walter, P., and Ron, D. (2011). The unfolded protein response: from stress pathway to homeostatic regulation. Science *334*, 1081-1086.

Wang, M., Ye, R., Barron, E., Baumeister, P., Mao, C., Luo, S., Fu, Y., Luo, B., Dubeau, L., Hinton, D. R., and Lee, A. S. (2010). Essential role of the unfolded protein response regulator GRP78/BiP in protection from neuronal apoptosis. Cell Death Differ *17*, 488-498.

Wang, X., Olberding, K. E., White, C., and Li, C. (2011). Bcl-2 proteins regulate ER membrane permeability to luminal proteins during ER stress-induced apoptosis. Cell Death Differ *18*, 38-47.

Wegorzewska, I., Bell, S., Cairns, N. J., Miller, T. M., and Baloh, R. H. (2009). TDP-43 mutant transgenic mice develop features of ALS and frontotemporal lobar degeneration. Proc Natl Acad Sci U S A *106*, 18809-18814.

Yoo, B. C., Krapfenbauer, K., Cairns, N., Belay, G., Bajo, M., and Lubec, G. (2002). Overexpressed protein disulfide isomerase in brains of patients with sporadic Creutzfeldt-Jakob disease. Neurosci Lett *334*, 196-200.

Zhao, F., Edwards, R., Dizon, D., Afrasiabi, K., Mastroianni, J. R., Geyfman, M., Ouellette, A. J., Andersen, B., and Lipkin, S. M. (2010). Disruption of Paneth and goblet cell homeostasis and increased endoplasmic reticulum stress in Agr2-/- mice. Dev Biol *338*, 270-279.

Zhao, L., Longo-Guess, C., Harris, B. S., Lee, J. W., and Ackerman, S. L. (2005). Protein accumulation and neurodegeneration in the woozy mutant mouse is caused by disruption of SIL1, a cochaperone of BiP. Nat Genet *37*, 974-979.